TAMPEREEN TEKNILLINEN YLIOPISTO
TAMPERE UNIVERSITY OF TECHNOLOGY

TONI MONTONEN

MULTIMODAL OPTICAL 3D-IMAGING SYSTEM - HARDWARE AND SOFTWARE

Master's Thesis

Examiners:
Professor Jari Hyttinen,
postdoctoral researcher Edite Figueiras
Examiners and topic approved in Faculty Council of the Faculty of Computing and Electrical Engineering meeting on June 3rd 2015

ABSTRACT

TONI MONTONEN: Multimodal optical 3D-imaging system: hardware and software
Tampere University of Technology
Master of Science Thesis, 55 pages, 5 Appendix pages
May 2017
Master's Degree Programme in Electrical Engineering
Major: Biomedical Engineering
Examiners: Professor Jari Hyttinen and postdoctoral researcher Edite Figueiras

Keywords: Imaging, three dimensional, tissue, hydrogel, cells, microscopy

Imaging technologies for three-dimensional (3D) analyses are needed for acceleration of progress in the tissue engineering (TE) research. The imaging methods that are available do not provide adequate information required for the assessment of TE products or they are destructive to the tissue. The optical imaging methods provide a low damage and high resolution solution. By merging different methods, their advantages can be combined and more information about the sample will be obtained.

The aim of the thesis was to develop and build a multimodal imaging system to examine the structure and function of TE constructs. To quantify the properties of a tissue-engineered graft, we need to see how the cells are organized in the graft and how the tissue functions. Hydrogels offer a non-opaque 3D culturing platform to be imaged with optical imaging methods.

The optical 3D imaging methods considered for TE research included optical projection tomography (OPT) and single/selective plane illumination microscopy (SPIM). These imaging methods are well suited for mesoscopic scale (1mm - 10mm) presented by the TE products while offering information of the cell structure on anatomical and fluorescence level. A custom multimodal imaging system combining OPT and SPIM was developed and built during this thesis. Furthermore, a control program was coded for controlling the system.

By taking advantage of the optical properties of hydrogels, live 3D high-resolution imaging of TE samples was attained with an OPT-SPIM setup. The cell distribution in the scaffold was obtained with bright-field OPT, and the fluorescence information was obtained with SPIM. The built system is capable of capturing very fine detail in the sample, the lateral resolution being under 1µm. The major advantage of this setup is the possibility of imaging the sample for extended periods of time through the stages of cellular development within hydrogels. This is enabled by the non-destructive nature of both imaging methods. Moreover, it is possible to gain information for further development of hydrogels as scaffolds for cell research and for graft validation before implantation.

TIIVISTELMÄ

TONI MONTONEN: Multimodal optical 3D-imaging system: hardware and software
Tampereen teknillinen yliopisto
Diplomityö, 55 sivua, 5 liitesivua
Toukokuu 2017
Sähkötekniikan diplomi-insinöörin tutkinto-ohjelma
Pääaine: Biolääketieteellinen tekniikka
Tarkastaja: professori Jari Hyttinen ja tutkijatohtori Edite Figueiras

Avainsanat: kuvantaminen, kolmiulotteinen, kudos, hydrogeeli, solut, mikroskopia

Kolmiulotteiseen analyysiin kykeneviä kuvantamismenetelmiä tarvitaan kiihdyttämään kudosteknologisen (KT) tutkimuksen edistymistä. Käytettävissä olevat menetelmät eivät tarjoa riittävästi tietoa KT-tuotteiden arvioimiseen tai vahingoittavat tutkittavaa kudosta. Optiset kuvantamismenetelmät tarjoavat näytettä vaurioittamatonta ja korkean resoluution tarjoavaa ratkaisua. Käyttämällä eri menetelmiä samassa järjestelmässä, niiden hyvät puolet voidaan yhdistää lisätiedon saamiseen näytteestä.

Työ tavoitteena oli kehittää ja rakentaa multimodaalinen kuvantamisjärjestelmä KT-näytteiden rakenteiden ja toiminnan tutkimiseen. KT-siirteiden ominaisuuksien määrittämiseksi on tärkeä nähdä kuinka solut ovat järjestäytyneet ja kuinka kudos toimii. Hydrogeeli toimii läpinäkyvänä 3D-viljelyalustana, jonka sisälle voidaan kuvata optisilla kuvantamismenetelmillä.

Optiset 3D-mikroskopiamenetelmät, joita harkittiin KT-tutkimukseen, ovat optinen projektiotomografia (OPT) sekä yksitasovalaisumikroskopia (SPIM). Nämä kuvantamismenetelmät sopivat hyvin mesoskooppisen mittakaavan (1mm-10mm) omaavien KT-näytteiden kuvantamiseen, samalla tarjoten solurakenteista anatomisella ja fluoresenssitasolla. Multimodaalinen kuvantamisjärjestelmä, joka yhdistää OPT:n ja SPIM:n, kehitettiin ja rakennettiin tämän työ aikana.

OPT-SPIM-järjestelmällä pystyttiin kuvantamaan KT-näytteitä korkealla tarkkuudella hydrogeelien optisia ominaisuuksia hyödyntämällä. Solujakauma geelissä saatiin käyttämällä OPT:a ja fluoresenssi-informaatio taltioitiin SPIM:lla. Rakennettu järjestelmä kykenee taltioimaan hyvin pieniä yksityiskohtia lateraalisen resoluution ollessa alle 1µm. Tämän järjestelmän merkittävänä etuna on mahdollisuus kuvantaa näytettä pitkiä aikoja hydrogeelissä sen käydessä läpi eri kehitysvaiheita. Tämän mahdollistaa molempien kuvantamismenetelmien näytettä vaurioittamaton laatu. Lisäksi hydrogeelien toiminnasta on mahdollista saada lisätietoa niiden edelleenkehittämiseksi solututkimuksen ja kudossiirteiden kasvualustana ennen implantaatiota.

PREFACE

This Master of Science thesis was carried out in BioMediTech as part of the Human Spare Parts-project. The project was mainly funded by EU, TEKES and Academy of Finland.

First and foremost, I would like to sincerely thank both of my examiners Prof. Jari Hyttinen and Ph.D. Edite Figueiras for believing in me, even though the project was challenging.

A special thank you goes out to the 3D-imaging group for cheering me on: Ph.D. Students Mari Lehti-Polojärvi, Birhanu Belay and Olli Koskela. A heartfelt thank you to Ph.D. Student Julia Johansson for helping me out with whatever problem I might have had. Through this thesis, I have had the opportunity and pleasure to work with some of the most amazing people I have ever met, the people of Computational Biophysics and Imaging Group.

I would also like to thank Ph.D. Students Janne Koivisto and Kaisa Vuornos for providing the samples for this thesis.

And lastly, I would like to thank my partner Tarja and my family. I am here because of you. I love you all.

This thesis is dedicated to my Dad who did not have the opportunity to see me graduate.

In Tampere, Finland, on 24th of May 2017

Toni Montonen

CONTENTS

LIST OF SYMBOLS AND ABBREVIATIONS

2D	Two Dimensional
3D	Three Dimensional
c	Speed of Light in Vacuum
c_m	Speed of Light in Medium m
CCD	Charge-Coupled Device
CMOS	Complementary Metal Oxide Semiconductor
FEP	Fluorinated Ethylene Propylene
FOV	Field of View
FWHM	Full Width at Half Maximum
hASC	Human Adipose Stem Cell
LED	Light Emitting Diode
MB/s	Megabytes per Second
µCT	Microscopic Computed Tomography
µMRI	Microscopic Magnetic Resonance Imaging
ND	Neutral Density
NIR	Near-Infrared
OCT	Optical Coherence Tomography
OPT	Optical Projection Tomography
RAID	Redundant Array of Independent Discs
sCMOS	Scientific Complementary Metal Oxide Semiconductor
SIM	Surface Imaging Microscopy
SPIM	Single/Selective Plane Illumination Microscopy
SSD	Solid-State Drive
TE	Tissue Engineering
UI	User Interface
UV	Ultraviolet

1. INTRODUCTION

The modern medicine needs novel techniques for the regeneration, replacement and repair of lost or damaged tissues. Research in the fields of TE and regenerative medicine is concentrated on finding solutions to restore tissue function and structure. These approaches typically involve a combination of biomaterials and cells. The interface between cells, biomaterials and tissue create an environment in which it is difficult to monitor and assess the final outcome of the TE therapy. [1]

Imaging technologies for three dimensional (3D) analyses are needed for acceleration of progress in the TE research. There is a great demand for a 3D imaging method that allows quantitative analysis of engineered tissue without damaging the sample. The imaging methods that are available do not provide adequate information required for assessment or are destructive to the tissue.

All imaging modalities require interaction with the sample, be it electromagnetic or mechanical energy. The sample will cause changes to the energy by refraction, absorption and scattering. These changes are measured to create an image of the sample. The type and frequency of energy will affect the achieved imaging depth, contrast and spatial resolution.

There is no commercial system in the current market for imaging TE products during various developmental stages. The confocal systems are not capable of imaging 3D hydrogel scaffolds at sufficient depths and SPIM system doesn't have the bright-field imaging option. OPT is not available commercially at the time of writing.

This thesis will concentrate on the optical 3D imaging methods that can be utilized for imaging TE products. Optical imaging covers the wavelengths of infrared (700nm-1mm), visible (380nm-700nm), and ultra-violet light (10-300nm). The optical imaging methods provide a low damage and high resolution solution for imaging the TE products in 3D. There are multiple different optical imaging methods capable of 3D imaging, like OPT and SPIM. Especially OPT has been used for TE product and hydrogel imaging and characterization [2]. However, OPT has clear limitations in fluorescence mode due to illumination of the whole sample while imaging and SPIM does not have bright-field capability When these different methods are merged into a multimodal imaging system, the advantages of different methods can be combined and more information about the sample could be obtained.

The goal of this thesis is to design and build a multimodal microscope with biological sample environmental controls for imaging TE samples. In order to image living cells for long periods of time, the microscope needs to be designed to cause minimal amount of light damage to the sample and to be able to sustain the vital functions of the imaged cells. To be able to quantify the properties of the TE graft, we need to see how the cells are organized in the graft and how the tissue functions. The grafts can be grown in different scaffolds to create the needed 3D structure. Most of the scaffolds are opaque and difficult to image without killing the cells that grow in the scaffold. Hydrogels offer a non-opaque 3D culturing platform for TE products. By having a non-opaque scaffold the optical imaging methods can be used to image the sample inside the scaffold. For best results, the sample also needs to be non-opaque to allow the light to travel through the cells. The aim for the developed setup is to be able to monitor cell migration, proliferation, differentiation and interaction inside hydrogel based TE products. The collected information will be processed and converted into better TE products in the future.

The actual designing of the system consists of two parts: software to control the microscope and planning the physical microscope. The microscope will be built around the specifications given by the biologists. This makes the microscope highly specific to the samples being imaged, in this case the TE products in hydrogel scaffolds. The program, however, should be as modular as possible to be easily exportable to other multimodal systems that use the same imaging methods but with different specifications. The backbone of the program should be robust enough to be modified for different imaging modalities.

Before building the system, the included imaging methods need to be considered. The idea is to have two methods that complement each other and, if possible, use the same components on some parts of the system. This keeps the cost and complexity of the system to a minimum.

On summary this thesis aims to combine SPIM and OPT with common control software with a design that allows combining of incubator for the cell culturing. The constructed system was tested for technical quality with real hydrogel and cell samples to assess its capability to image TE constructs.

2. BACKGROUND

2.1 Light Properties

What we call light is a narrow band of wavelengths in electromagnetic spectrum. Light used in this context consists of visible light and wavelength areas close to visible spectrum, for instance near infrared (NIR) and ultra violet (UV). This area of light ranges from 100nm up to 1400nm. [3]

As electromagnetic radiation, light can be described from quantum or classical view point. Classical theory considers light as an electromagnetic field consisting of continuous range of energies while quantum model describes light as packets of energy called photons. Both models are necessary when considering light interaction with matter. Classical model is utilized in scattering calculations and quantum model is used as part of absorption and luminescence calculations. [3]

2.2 Optical Imaging Microscopy in Three Dimensions

Optical microscopy was invented around the 17th century and it has remained an important part of biological study to this day. The basic design of an optical microscope is simple. It uses visible light and lenses to magnify images of small objects. Detection of the image can be achieved by eye, photographic film or camera. Modern complementary metal oxide semiconductor (CMOS) and charge-coupled device (CCD) cameras have made the other detection methods mostly obsolete and images are saved digitally to a computer removing the need for eyepieces. [4]

Conventional microscope is good for examining the surface of the sample. Problems arise when sample needs to be imaged from inside or under the immediate surface. Mechanical sectioning has been used to slice the sample into thin slices for imaging the inner structure. This is adequate for fixed samples but living samples will always get damaged during mechanical sectioning. Modern scientists are interested in seeing inside the sample while it is still living and novel imaging methods have been created to answer this demand. [5]

Optical imaging methods provide a low damage and high resolution solution for imaging in 3D. When imaging living samples it is important to cause as little damage as possible to the imaged sample. The advantages of optical imaging compared to other radiological imaging methods in this context are numerous. Optical imaging covers the wavelengths of infrared (700nm-1mm), visible (380nm-700nm), and ultra-violet light (10-300nm). These wavelengths are non-ionizing radiation and create images by exciting the electrons

in the sample without the damage caused by ionizing radiation used by many other imaging methods. [6] This enables imaging of live samples for even longer periods of time and duplicating the procedure for the same sample if needed [5]. Optical imaging is particularly suitable for soft tissue imaging due to differences in tissue absorption and scattering of light. Various wavelengths of light can be used to analyze or measure different properties of tissue simultaneously. [6] This makes optical imaging very suitable to be used with TE products.

While the most common 3D imaging methods used to image cells in biosciences are widefield fluorescence microscope and laser scanning fluorescence microscope in all its forms (spinning disc, two-photon, etc.), they cannot be used to image large 3D volumes due to light scattering in the specimen. They are limited to the surface depth of around 200µm. Other optical methods have been implemented for mesoscopic 3D volumetric imaging. The light-optical methods include: surface imaging microscopy (SIM), optical coherence tomography (OCT), OPT, as well as SPIM. In addition, non-optical methods like microscopic magnetic resonance imaging (µMRI) and microscopic computed tomography (µCT) offer potential solution to collecting 3D data from mesoscopic samples. [7]

One of the requirements of 3D imaging of the mesoscopic samples is the possibility to optically section the sample from multiple imaging depths in the range of hundreds of micrometers to several millimeters. None of the aforementioned imaging methods can address all the requirements of TE samples. Non-optical methods can not compete with the resolution of the optical methods and are therefore left out of this evaluation. SIM is destructive to the sample, sectioning the sample physically to obtain 2D images that are later assembled into a volumetric reconstruction. [7] OPT and OCT rely on tomographic approach, both employing different approach to obtain the volumetric data from the sample. OPT transilluminates the sample and captures images from different sample orientations while OCT relies on reflections to derive the depth information [8][9]. SPIM generates 2D slides using orthogonal laser light sheet to activate fluorophores at the focal plane of the camera [10].

In optical 3D imaging a 3D model is normally created from a multiple 2D images taken from a sample. In addition to the 2D image, the creation of 3D conversion requires information about the location, direction and/or distance of every 2D frame in relation to every other 2D frame. Images are taken with a CMOS or CCD camera to be reconstructed into a 3D image on the fly or saved for later analysis. 3D image reconstruction can be done in the microscope or with an external program. [11]

2.3 Light Propagation in Tissue

When light is propagating through a substance with cells or tissue in it, there will be three photophysical effects affecting the light: refraction, scattering, and absorption. These ef-

fects will be the basis in creating the image of the sample. With transilluminating microscopes the dynamics in the image are created by all of the mentioned photophysical effects creating a shadow on the photodetector while fluorescence based microscopes rely on absorption to excite fluorophores and the emitted light created when the return to relaxed state.

2.3.1 Refraction

Usually the linear optical properties of the material are described by a constant known as refractive index.

$$n(\lambda) = \frac{c}{c_m(\lambda)} \tag{1}$$

The refractive index is defined by a speed of light in vacuum (c) compared to the speed of light in the medium (c_m). The speed of light in the medium is also related to the wavelength of the light. [3]

When a light wave is propagating through a material with a given refractive index and it encounters a boundary of material with different refractive index, the propagation direction of the light will change. Depending on the refractive index difference and the angle of incidence at the boundary, refraction and reflection result. Snell's law describes the relation between the angle of incidence and angle of refraction:

$$sin\theta_2 = \frac{n_1}{n_2} sin\theta_1 \tag{2}$$

Where angle of incident is θ_1 and angle of refraction is θ_2. This is show in Figure 1. [3]

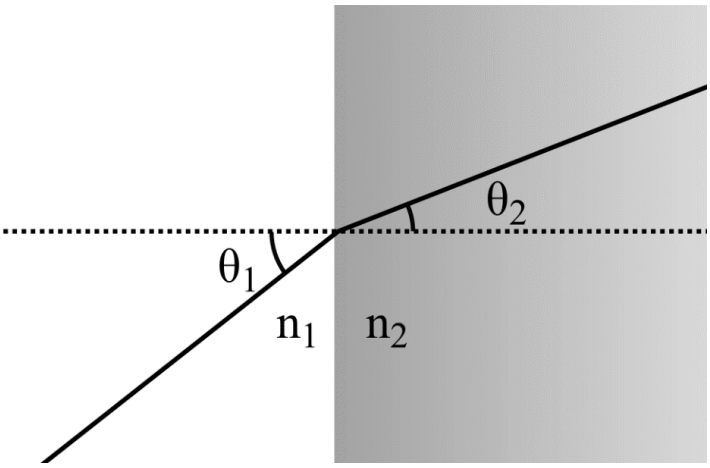

Figure 1. *Refraction happens at the boundary of two optically different materials. θ_1 is the angle of incidence, θ_2 is the angle of refraction and n_1 and n_2 are the refractive indices, with $n_2 > n_1$.*

2.3.2 Scattering

When there is only a small volume of foreign material inside host material, scattering of light will occur. In tissue samples, the different layers and organelles in cells will cause scattering. Scattering causes the light to be redirected across a range of angles relative to scattering particle. Scattered power can be calculated with formula:

$$P_{in} = P_{scatt} + P_{out} \tag{3}$$

$$P_{in} = I_0 A \tag{4}$$

$$P_{scatt} = I_0 \sigma_s \tag{5}$$

$$P_{out} = I_0 (A - \sigma_s) \tag{6}$$

Where I_0 is the intensity of the beam, A is the area of the beam, and σ_s is the area of the scatterer. [3]

Scattering can be divided into three different categories depending on the size of the scatterer: Rayleigh limit, Mie regime, and the geometric limit. Rayleigh limit is considered when the scatterer is smaller compared to the wavelength of the incident light. Mie regime is in effect when the scatterer is in the same region regarding the wavelength. The geometric limit occurs when the scatterer is larger than the wavelength of the incident light. [3]

2.3.3 Absorption

Absorption is a process where a molecule in the material reduces the power of light beam it is in contact with. This energy transfer causes the molecule to enter to a different energy level in a phenomena known as transition. For the transition to occur, the molecule needs to absorb energy comparable to the difference of the energy levels according to the formula:

$$hv = \Delta E \tag{7}$$

Where ΔE is the difference in energy between two levels and hv is the energy of a photon. [3]

The absorption is the basis for the fluorescence microscopy: the fluorescent molecule, fluorophore, absorbs a photon and gets excited. This fluorophore then returns to the stable state and emits a photon with lower energy compared to the absorbed photon. [7]

2.3.4 Principles of Fluorescence

Some of the microscopy methods utilize the use of fluorescents to form the image. Fluorescents are molecules that emit light after excitation by mechanical, physical or chemical mechanism [12]. This emitted light can then be observed at the detection end and image formed accordingly. Fluorescents have helped in circumventing the classical limitation of optical microscopy: according to Nyquist-Shannon sampling theorem, it is impossible to obtain better resolution than half the wavelength of light. The Nobel prize in chemistry 2014 was awarded jointly to Eric Betzig, Stefan W. Hell and William E. Moerner *"for the development of super-resolved fluorescent microscopy"* [13]. Their work with fluorescents and high-resolution microscopy brought the optical microscopy into the nanodimension.

Fluorophores are used to stain the desired parts of a sample for fluorescence imaging. Fluorescence imaging had a major breakthrough when cloning of green fluorescent protein (GFP) succeeded in 1992 [14]. This made biological labeling of cell structures, proteins and dynamic processes inside living cell structures possible. Since then more fluorophores have been discovered on a monthly basis and fluorescence has become the backbone of live cell imaging. Fluorophores can be divided in three main groups: fluorescent labels, fluorescent indicators, and genetically expressed fluorescent indicators. These groups are utilized in different imaging conditions and can even change their fluorescence properties in response to specific physiological parameters. [7]

The fluorescent molecule can be deliver to the sample in multiple different ways from direct permeability (Live/Dead staining) to the sample producing the fluorescent protein

itself (Green fluorescent protein production). The staining procedure depends on the imaged sample and the selected fluorophore. [7]

In microscopy, the fluorescents are usually excited by exposing them to light. When a fluorophore absorbs a photon, it enters an excited state. The excited molecule will then return to a relaxed state by releasing a lower energy photon (compared to the absorbed photon) and heat. Different fluorescents have different qualities regarding their excitation and emission wavelengths. However, the emitted light is always of higher wavelength compared to the excitation wavelength. This effect is called Stokes shift. [7]

Thus, the emitted light is collected by the detection optics to create an image. In contrast to the conventional microscope, fluorescence microscopes can have a very high resolution and the most accurate ones are capable of imaging even single molecules because of the properties of fluorescence emission [12].

2.3.5 Photobleaching and Phototoxicity

When imaging with fluorophores there are some limitations to how long a sample can be illuminated before the fluorescence molecules stop emitting light. This phenomenon is known as fading and it is caused by photobleaching. Photobleaching means irreversible chemical changes in the fluorescent molecules prohibiting its ability to fluoresce [15]. The longer the sample is exposed to light the weaker the emitted signal gets thus lowering the signal-to-noise ratio [7]. Avoiding photobleaching is one of the major concerns when building a system for live cell imaging. To avoid cell damage and photobleaching correct imaging methods need to be implemented to the system. Photobleaching is not always an unwanted effect. There are imaging methods that are based solely on photobleching, such as fluorescence recovery after photobleaching (FRAP). However, in the scope of this thesis, photobleaching was avoided.

Phototoxicity is also a major concern when imaging live cells. All live cells suffer under light exposure and this can even lead to cell death if the amount of light absorbed goes over the tolerance level of cells. Phototoxicity is caused by exciting light and fluorescent emission. Most of the damage comes from direct exposure to the exciting light. This light can, however, scatter and cause damage also to the cells that are not in direct exposure. Even the fluorescent emission light will cause phototoxicity to the adjacent cells. [16]

To reduce the effect of photobleaching and phototoxicity the intensity of the exciting light should be kept as low as possible. This causes problems with the image quality because less light is illuminating the sample and therefore fever fluorophores are being excited. This in turn causes less emitted light and lower signal-to-noise ratio. There is always a trade-off between image quality and damage caused to the imaged sample. [17]

2.3.6 Resolution of Optical Systems

The finite aperture of non-ideal objective causes diffraction pattern limiting the performance of a real optical system. If a point source is inspected through this optical system, a bright spot with concentric rings of reducing intensity is observed. The spot is called Airy disc. [18]

The resolution of a real system is defined by the distance between two point sources while they can still be resolved as two separate point sources. There are multiple different criteria for the distance, but the most widely used is the Rayleigh's criterion. This defines that the two points are separate if the distance between points is:

$$r = \frac{1{,}22\lambda}{2n\,sin\theta} = \frac{0{,}61\lambda}{NA} \tag{8}$$

where r is the minimum resolvable distance between the two points, λ is the used wavelength, θ is the half angle of light entering the objective, n is the refractive index of the media, and NA is the numerical aperture of the objective.[18] The distance r is also the first dark ring around the Airy disk. If two points are separated by distance given by Rayleigh's criterion, the area between the center intensities will be 26% dimmer than the peaks. The Rayleigh's criterion is demonstrated in Figure 2. [7]

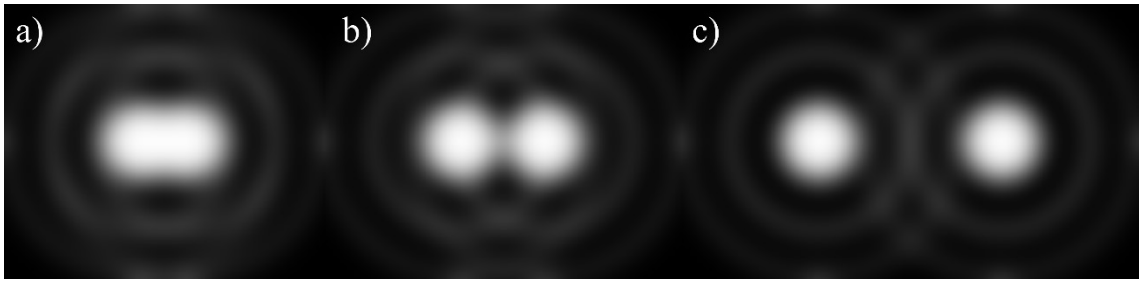

Figure 2. *Rayleigh's criterion. a) Two points are closer than Rayleigh's criterion, they can not be distinguished. b) Two point are exactly Rayleigh's criterion apart and can be differentiated. c) Two points are more than Rayleigh's criterion apart and are clearly separate points.*

2.4 Selective Plane Illumination Microscopy

Light-sheet microscopy has gained a lot of interest in recent years. It was chosen the method of the year 2014 by Nature Methods [19]. Multiple different light sheet configurations have been built with a specific imaging goal in mind. One of those is SPIM [10]. SPIM is an emerging new imaging method in the field of biomedical imaging. It is a fluorescent-based imaging method capable of creating 3D images of millimeter-sized samples. It has already risen as one of the most promising new methods because it causes very low amounts of photobleaching and phototoxicity to the imaged sample allowing

time lapse imaging of live samples. This is one of the reasons SPIM was chosen as one of the modalities of the imaging system.

SPIM was introduced to the life sciences in 2004 [10]. It was based on the idea of using a light sheet to achieve optical sectioning proposed already in 1902 [20], and refined the idea of macroscopic biological specimen imaging published in 1993 [21]. SPIM answered the need for an imaging method capable of single cell resolution and deep penetration combined with fast acquisition speed. This need was created with the invention of genetically encoded fluorescent proteins in 1992 [14]. Scientists could stain different cell types in living organisms, but no imaging method available at the time could answer the speed and penetration demands to capture all the details in a living embryo. The size and the opacity of the embryos (>1mm) meant that no other method could be used to image the whole organism and achieve single-cell resolution also in the deeper tissue areas. With reduced photo-toxicity compared to other imaging methods available, fast image acquisition and flexible sample orientation, SPIM excels at imaging live samples. It is ideal for imaging rapid developmental processes in cells, tissue samples or even entire animals.[22]

2.4.1 Principles of SPIM

Optical sectioning in SPIM is achieved by illuminating the sample along a separate optical path orthogonal to the wide-field detection path as shown in Figure 3. The excitation light is focused by a cylindrical lens that creates a sheet of light that illuminates only a thin area of the sample. This area is the focal point of the detection optics so only the area of the sample that is in focus is illuminated. Therefore, no out-of-focus excitation is generated removing the need for the pinhole system used in confocal microscopy. Additionally, the whole image area of detection camera is illuminated simultaneously enabling fast image capture and reduced bleaching. By separating the illumination path from the detection path, photo toxicity is only caused to the light sheet illuminated plane. This lowers the total damage caused to the sample by the factor of $N\text{-}1$, where N is the number of imaged planes, because each plane is only exposed once during a stack [10]. The thickness of the light sheet is usually much thinner than the depth of field of the detection objective which means that the thickness of the light sheet defines the axial resolution.

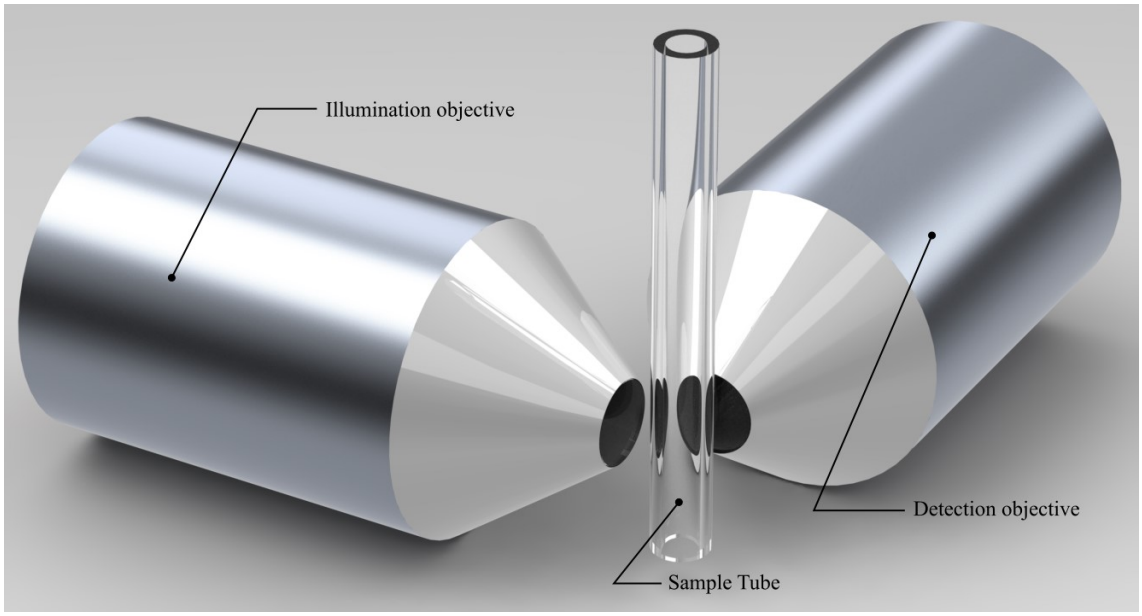

Figure 3. *The illumination and detection objectives are oriented orthogonally. The sample tube can be rotated and moved in X-Y-Z-axis.*

2.4.2 Optic Design of SPIM

The optical arrangement of a SPIM is straightforward although different from conventional wide-field fluorescence microscope. The detection path is almost always identical to that of conventional microscope: A detection objective to collect the light emanating from the sample and a tube lens to project the light on a camera sensor. Detection path may also include a detection iris, an emission filter and in some cases even a dichroic mirror to divide the signal for several cameras. In the most common setups there is no need for dichroic mirror because the illumination and detection paths are separated. In SPIM the illumination path is orientated orthogonally to the detection path. It consists of a coherent light source, lenses and mirrors to guide the collimated light beam, cylindrical lens to create a light sheet out of the light beam, slits to shape the sheet and illumination objective to project the light sheet to the sample chamber. Illumination path may also include resonant scan mirrors to create a pivoting light sheet [23] or remove the need for some lenses and mirrors by using optical fiber to transport the light beam. Even though the optical arrangement of the illumination path may vary, the complex interactions between different optics in the illumination path mean that the position of every optic is crucial to the creation of the light sheet. The components used to create the light sheet may vary between different SPIM systems.

In order to obtain the best quality images, a medium filled sample chamber fitted with water-corrected illumination and detection objectives combined with a water-based sample mounting to create a refractive index-matched beam path. The medium filled sample

chamber also allows the imaging of live samples for longer time periods by enabling the use of incubation system to provide the sample with nutrition and oxygen. This creates an environment that enables the survival of the sample for days. This is a very important aspect if imaging concentrates on the developmental biology like embryos. [24]

The sample is mounted inside hydrogel in a sample tube. Depending on the sample the hydrogel can be tailored to allow sample movement and growth. If the hydrogel is thick enough the sample can be pushed out of the tube to avoid aberrations to the final image from the tube walls. Usually, the tube is chosen so that the material has a refractive index close to water, for instance fluorinated ethylene propylene (FEP) tubes. [25]

Light sheet microscopes including SPIM are usually set up horizontally because of the orthogonal optical arrangement. Because the optical arrangement is fixed and the sample needs to be at the intersection of the illumination and detection paths, the simplest way is to hang the sample from above and move it along the optical axis of the detection system through the illumination plane to acquire stack of images. This means that the sample chamber can be open-topped and filled with medium while only the objectives need to be sealed to waterproof the sample chamber. Another benefit of the vertical sample mounting is that the sample can be rotated around its axis without deformations and to image the sample from multiple angles [26]. A combination of linear and rotational stages is used to focus an area of interest in the sample and to record z-stack, multi-position and multi-view datasets.

2.4.3 Performance of SPIM

The performance of a SPIM system depends on multiple factors but one of the most important is the light sheet. Properties of the light sheet are usually customized according to the intended use of the microscope. Light sheet should be designed to be as thin as possible and uniform across the field of view. The shape of the light sheet depends on the numerical aperture of the illumination objective creating a thin light sheet for small fields of view or thicker light sheet for large field of view [27]. In the case of imaging live specimens it is better to use water-dipping objectives to minimize the amount of interfaces with different refractive indexes the light sheet has to cross because the specimen is usually imaged in a medium filled chamber. This creates the optimal light sheet across the entire spectrum.

One of the advantages of SPIM is that it can be used to image a sample with high resolution for longer periods of time, even days. This means that the data sets get enormous because the acquisition speeds can be very high, several gigabytes per minute, as shown in Fig. 5. Modern cameras are capable of taking high resolution (2048x2048) images at a very fast rate (>100 images per second). This means that the SPIM system demands very fast data storing. A large work memory (64Gb) with large SSD-drives in RAID-mode are the minimum requirements of the computer to use its full potential. Even this kind of

advanced setup can run out of storage space really quickly. Thus, the speed the samples can be imaged with is no longer limited by the acquisition but by the data handling: processing, data storage, and data transfer. [28]

Comparing SPIM with its closest competitors, confocal microscopy and 2-photon microscopy, reveals that SPIM causes a lot less damage to the imaged sample as shown in Figure 5. In confocal and 2-photon microscopes the areas in front and behind the imaged plane are also illuminated causing unnecessary bleaching and phototoxicity. This extra exposure to the light can cause the sample to suffer irreversible damage. Although 2-photon microscopes activate only the fluorescents in the focal spot, the illuminating light in both confocal and 2-photon microscopes goes through the sample across areas not being imaged causing damage to the cells. This damage can also cause significant changes to the development of imaged cell clusters, for instance embryos [16][17]. The longer wavelengths of light the 2-photon systems use causes less damage to the sample compared to the shorter wavelengths used by SPIM and confocal microscopy mitigating the effects of out of focus illumination [29].

Resolution of these systems can be compared in lateral and axial directions. In lateral direction, the confocal microscope has higher resolution while SPIM reaches the same resolution as wide-field systems. However, in axial direction the resolution of SPIM improves drastically due to the nature of light sheet illumination and offers over 4 times better resolution when compared to confocal microscopes while using low magnification objectives (5x). This advantage is lowered when using higher magnification objectives (40x, 100x) but even with high magnification objectives SPIM has at least equal axial resolution than confocal microscopes [26]. Because the resolution of a microscope system scales inversely with the wavelength used, 2-photon microscopy suffers from the long wavelength it uses to illuminate the sample giving it approximately half the resolution of confocal systems. [30]

While the resolution and phototoxicity are two of the most important aspects while imaging living samples, the imaging speed should not be overlooked. SPIM saves a frame of the whole field of view at the same time while confocal and 2-photon microscopes need a scanning mechanism to image a certain area of the sample. This takes more time than saving a single frame. This means that confocal and 2-photon microscopes are confined to the speed of the rastering mechanism, fluorescent activation, and detection of emitted fluorescence signal pixel by pixel. This limits the imaging speed of confocal and 2-photon microscopes to a fraction of the speed of SPIM system. Because a SPIM system illuminates the whole image plane at the same time, all the fluorescence is activated at the same time and emitted fluorescent light from this plane is detected in one frame by the camera. SPIM can be used to image dynamic movement in 3D, for instance beating heart [31] or cell migration during embryogenesis [32].

One of the limiting factors for the performance of a SPIM system is the optical properties of the imaged sample as shown in Figure 4. Irregularities or opaque areas in the sample will cause absorption, reflection and refraction of light and thus affect the quality of the light sheet. The non-uniform light sheet will in turn cause stripes of shadows or blurred areas to the end-image. This can be corrected by implementing a second illumination path to the system (mSPIM) [23]. The second illumination path is usually identical to the first path but illuminates the sample from the opposite direction. Both of the sheets are aligned to the same focal plane. The second light sheet decreases some of the negative effects caused by the optical defects in the sample like shadow stripes. The positive effect on the image quality can be amplified by using additional optics in the illumination paths to create a pivoting light sheet [23].

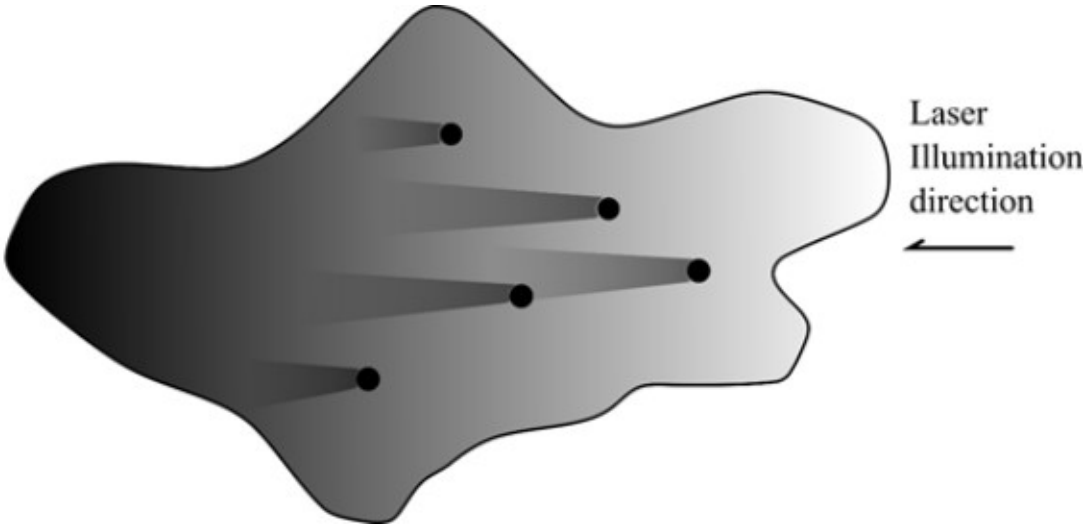

Figure 4. *One sided illumination in conventional SPIM results in shadows and attenuation behind optically denser parts of the sample.*

In case of some samples even the double sided illumination is not sufficient, for instance embryos. The sample is excessively opaque and it will deform the light sheet as well as absorb the light emitted by the fluorophores. Therefore, the sample must be rotated and imaged from several directions to increase the quality of the image. Alternatively a second detection path can be implemented to the opposite side of the sample [33]. When these overlapping images, obtained either from rotation or second detection path, are processed, the result is a more isotropic resolution [34].

Another drawback of SPIM, confocal microscope and 2-photon microscopy is their ability to image only fluorescent samples. While fluorescents help define and characterize different parts of the sample, it is really difficult to analyze the images in context of the whole sample. This drawback can be overcome by combining OPT technique with SPIM. This can be achieved because in SPIM the illumination path is perpendicular to the detection path and does not share components with it. Therefore, the detection path can be used with other imaging methods to reduce the total cost of the system.

A) Point illumination (confocal microscope)

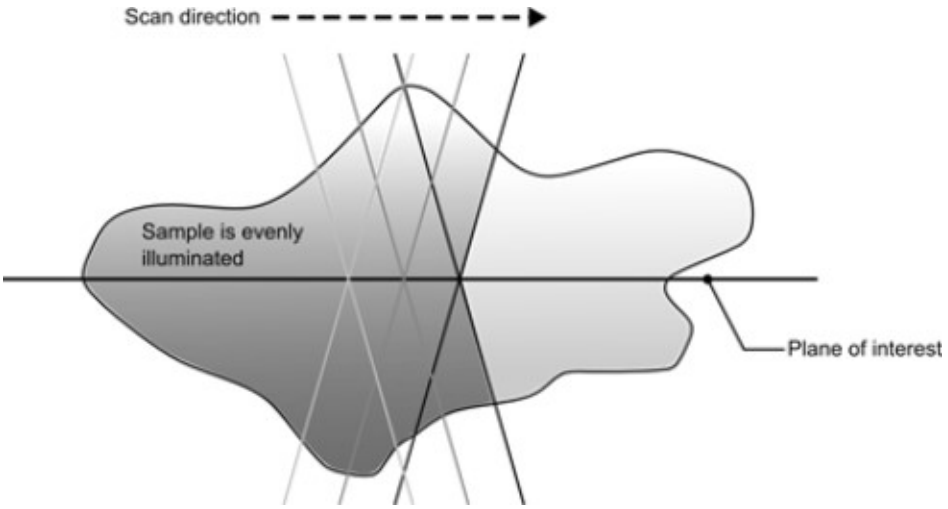

B) Plane illumination (SPIM)

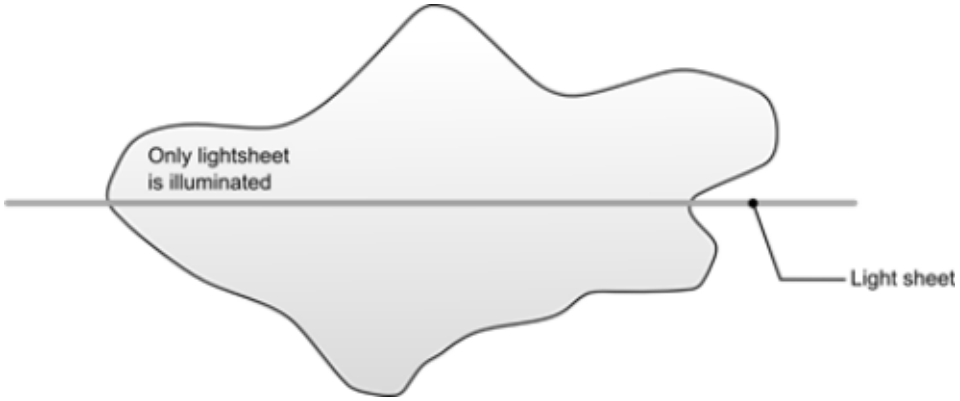

Figure 5. *SPIM compared to confocal microscopy A) Illumination in confocal microscopy covers the whole sample even when imaging only a single plane. B) Illumination in SPIM covers only the plane to be imaged.*

2.5 Optical Projection Tomography

OPT was developed in 2002 to image samples (sized ~1mm – 10mm) that could not be imaged efficiently with existing 3D imaging techniques, mainly magnetic resonance imaging (MRI) and confocal microscopy. OPT is capable of 3D imaging with both bright-field and fluorescent sources. It is based on the projection tomography used in other successful applications like medical computerized tomography (CT) in which x-rays are used

to project the image of the sample. In OPT the x-rays used in CT are replaced by light. This means that OPT does not have the negative effect of radiating the sample. [35]

2.5.1 Principles of OPT

There are two ways of creating images with OPT: emission OPT (eOPT) and transmission OPT (tOPT). Emission OPT is based on exciting fluorescents in the sample with light that is in the excitation area of the chosen fluorescent. Emitted light is then separated from excitation light with a chromatic filter. This is possible because the excitation wavelength is usually different to the emitted wavelength. Filtered light consisting only of emitted wavelengths is then collected with optics to a camera chip to create an image. Transmission OPT is simpler and is based on white light transmitted through the sample. The light is then collected to the camera chip and the shadows of the sample create an image. [36]

2.5.2 Optic Design of OPT

Like most microscopes, optical projection tomography system consists of three main parts: Illumination, detection and sample manipulation. All of the three main parts consist of multiple individual parts. Diagram of a typical tOPT setup is shown in Figure 6.

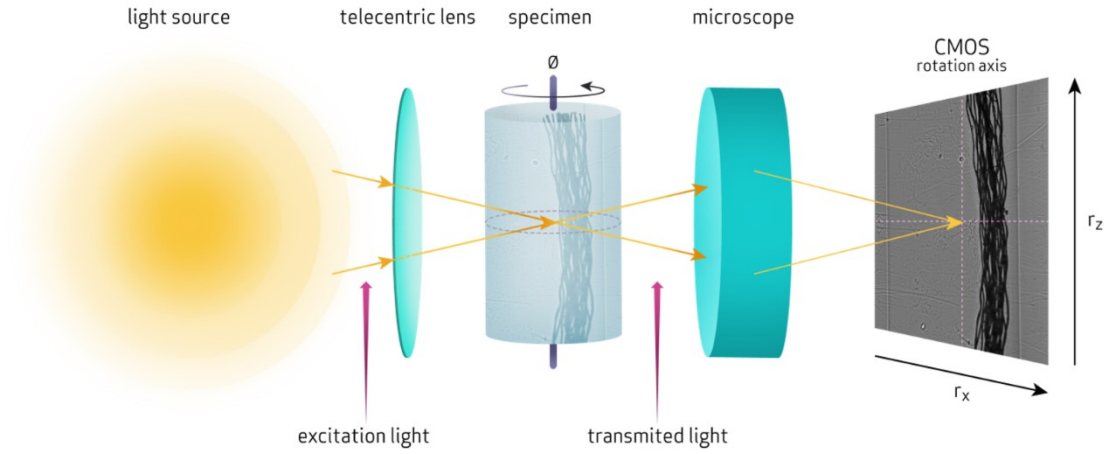

Figure 6. *Diagram of transmission optical projection tomography. Diffuse light passing through the sample is collimated by the microscope and recorded by a camera (CMOS). By rotating the sample images are captured from multiple angles.*

The illumination path consists of a light source and optics to collimate the light to the sample. The direction of the illumination changes between eOPT and tOPT. In eOPT the light comes from the same direction as it is detected and in tOPT the light comes from the opposite direction of detection. In order to get the best image, the illuminating light needs to cover the whole area to be imaged and the intensity of the illumination needs to

be as homogeneous as possible on this area. A diffuser is used to create this even intensity coverage. To get as much of the illumination to the sample, a collimator is used on the illumination path. The collimator is almost essential in the tOPT by making the illumination light parallel to the detection axis and thereby reducing the area of penumbra in the final image. Telecentric optics can be used as collimators and they add the advantage of the constant magnification through the sample [37].

The sample manipulation part of the system provides sample attachment and movement controls. Normally, the movement is motorized but also manual movement stages are usable. The x-, y-, and z-axis are controlled by linear stages, one for each axis. These can be manually controlled, because in normal OPT imaging no linear movement is needed. However, if movement is required, these stages need to be motorized [38][25]. Sample rotation is handled by a rotational stage. This has to be motorized and computer controlled for maximum precision. Usually the final 3D image is created from several hundred frames taken by rotating the sample 360 degrees around a single axis and taking a frame at constant intervals. The Rotational stage must have a x-y-stage attached to it to center the rotation axis to a feature in the imaged sample.

Detection path consists of detection objective, filters and pinhole if needed, and digital camera. The detection objective collects the light coming from the sample. This can also be telecentric to keep the magnification of the image constant regardless of the distance between the camera and the objective.

The objective defines the area of the sample that is in focus. The area in acceptable focus is called depth of field. Usually, this focal area is positioned so that it covers the region of the sample located between the rotation axis and the detection path as shown on Figure 7. Areas of the sample that are outside of depth of field end up being out of focus in the final image. This means that there is as little sample as possible between the focal plane and detection to cause issues in the end image. [39]

The filter is included if fluorescents are used to cut non-interesting wavelengths out of the detected light and to preserve the emitted light [36]. Pinhole is used to control the intensity of incoming light. This way the exposure time of the camera can be adjusted more flexibly. The camera itself is usually a CCD or a scientific CMOS (sCMOS) camera.

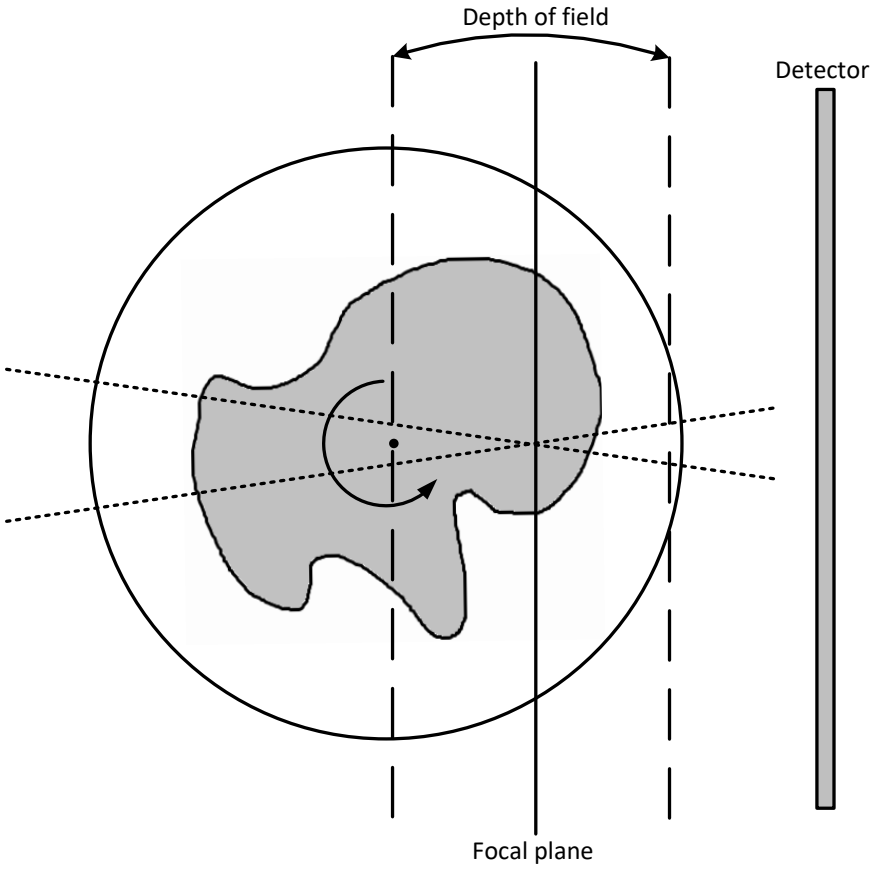

Figure 7. *The depth of field is positioned over the half of the specimen nearest to the detector*

The image is captured in OPT by a digital camera in order to increase detection efficiency and speed up the process. The CCD cameras used in most setups can take high amount of frames per second with high resolution. The parts before the camera on the detection path (objective, filters, and pinhole) are used to collect the light for the image creation.

2.5.3 Imaging with OPT

While the image captured with OPT is ready to be viewed as a single image straight away, the most useful feature is that OPT images can be combined into a 3D projection. In projection tomography the projections of the sample from different angles are used to create 3D model of the sample. In OPT this is handled by rotating the sample around its center axis and taking an image from as many directions as needed. The 3D data produced by projection tomography is not usable straight away like with sectioning tomography used in confocal microscopes. The data needs to be mathematically transformed to create a 3D model of the original sample by combining the information included in the different directional images.[8]

The sample is imaged in OPT by rotating it around a single axis and taking digital images from multiple positions. These images are then used to reconstruct virtual slices of the sample with back-projection algorithms. The two different imaging methods of OPT require different back-projection algorithms to create the final images. Images acquired in the eOPT represent the intensity of sources of fluorescence through the sample. In tOPT the darker parts of the image represent the light that was attenuated by more opaque parts in the sample. [39]

There is no direct comparison for OPT, it is a unique imaging method on its own. It causes very little damage to the imaged sample and is capable of fluorescent and bright-field imaging. Bright-field images of the sample create context for the fluorescent images by showing the surrounding tissue that has not been dyed with fluorescents. The main reason for including OPT to this system is this ability to create context for SPIM images [40]. It is convenient to fit OPT into the SPIM setup because the illumination paths are perpendicular to each other: OPT uses back illumination and SPIM uses side illumination. This combined with the fact that both imaging methods can use exactly the same detection path makes this combination particularly inviting.

3. MATERIALS AND METHODS

3.1 System Requirements

The system is designed for imaging TE product consisting of cells and hydrogel scaffolds. The resolution of one micrometer and under is required to be able to quantify the sample and scaffold. The sample is fragile to all damage and long imaging runs are needed. To take this into account, the imaging methods chosen for the multimodal system are very gentle to the sample. Optical 3D imaging methods we considered for TE research include OPT and SPIM. These imaging methods are well suited for mesoscopic scale (1mm - 10mm) presented by TE products while offering information of the cell structure on anatomical and fluorescence level.

Considering the samples to be imaged with the system, almost all samples will have a major component of water. This affects the quality of images if imaging modality is relying on visible light due to refractive index changes on the illumination and detection paths. In order to avoid mismatches in refractive indexes, the system needs to be designed to have water as an immersion liquid.

The objective of this thesis is to build a system capable of high-resolution 3D imaging of TE products and hydrogels without causing too much damage to the sample. The system is designed to be easy to use and stable. The design is centered on two modalities that give complimentary information of the imaged sample.

3.2 Determining the Needed Structures

The design of the system is based on the OpenSPIM-project [41]. It is an open-access platform for applying and enhancing the SPIM system. The site provides build instructions and help for scientists looking to build and use their own SPIM system. The system described in this thesis was created around the instructions provided in the site. However, the inclusion of the OPT in the system meant that the control software used in OpenSPIM could not be used. A custom program to control the functions of the system was created. Most of the components have been changed to accommodate the needs of our facility.

The structures and components needed to build the system are as follows:

- Laser
- Camera
- movement stages
    - Rotational
    - Linear

- Illumination light emitting diode (LED) for OPT
- Objective and optics for laser illumination path
- Objective and optics for detection path
- Components for sample chamber (need to be manufactured or 3D-printed)
- Components for sample holder (need to be manufactured or 3D-printed)
- Components for aligning light sheet with camera
- Components for perfusion incubation
- Computer to run the imaging program and save the data

These structures and components are mainly derived from OpenSPIM-site but the components for perfusion incubation are not included in the site. The sample chamber needs to be modified from the provided solution to include an opening on one of the walls for the lighting for the OPT transmission imaging mode. Other items and parts are chosen according to the future needs that the system might have. This means that the parts may differ from the parts given at the OpenSPIM-site.

3.2.1 Layout of the System

The layout of the system consists of three main paths: OPT illumination, SPIM illumination, and detection for both. The simplest path is the OPT illumination which consists of only the illumination LED system with telecentric lens. This creates the light needed for OPT imaging. The illumination path for SPIM creates a laser sheet needed for accurate activation of fluorophores in the focal plane of the detection objective. The detection path is designed to capture light from the detection objective and compiling that information into an image. The SPIM illumination path and the detection path are perpendicular while OPT illumination is parallel to the detection path. The layout is presented in Figure 8.

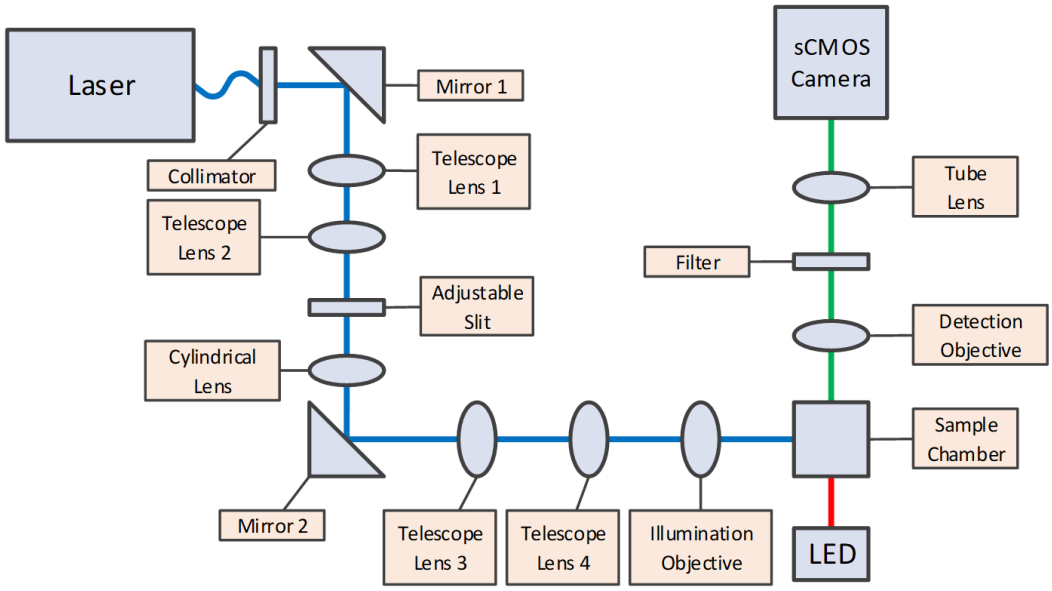

Figure 8. *Layout of the optical elements in the system. Blue line shows SPIM illumination path, red line shows OPT illumination path, and green light shows detection path for both modalities of the system.*

3.2.2 Components

The system needs to be applicable with the common dyes used in the cell biology methods. This created a demand for a laser that has specific wavelengths for the specific fluorescents. This kind of laser was custom built (Modulight, Tampere, Finland) to our specifications. It has 3 wavelengths (488nm, 561nm and, 635nm) for activating different fluorescents. Included wavelengths open up a possibility to image a wide variety of samples and structures depending on the needs of the current project. Laser is designed to be stable even at lower power settings (< 40mW). The low power is used to avoid photobleaching and phototoxicity to the imaged sample during longer periods of continuous imaging or time lapse imaging. The system was designed to have the possibility for interchangeable lasers by including collimating fiber port as a laser input. The reflective collimator gate (RC02FC-P01, Thorlabs Inc, Newton, New Jersey, USA) attached to a mirror mount is used to direct the laser beam to a mirror (POLARIS-K1 & BB1-E02, Thorlabs Inc, Newton, New Jersey, USA) that is used to align the beam accurately with the illumination path. The reflective collimator is the best collimation choice for the system because of multiple wavelengths used in the system. The off-axis parabolic mirror used in the reflective collimator has a constant focal length across wide wavelength range. This property of the collimator makes it ideal for applications with polychromatic light.

In order to get the optimal results from the system, the camera needs to have a resolution to create an image with all the information provided by the detection objective. This resolution is determined by the used wavelength and the numerical aperture (NA) of the

detection objective. This is calculated with Rayleigh's criterion in formula 8. The maximum resolvable resolution with the chosen objective and laser depends on the chosen laser wavelength. To distinguish two subresolution particles from each other, the particles need to be imaged in different pixels of the camera chip. In order to have two particles in different pixels, the maximum resolvable resolution (the distance between the two particles) should be the width of one empty pixel between objects. Considering the Rayleigh's criterion, this means that the intensity of the middle pixel should be 26% lower compared to the pixels containing particles. For the ideal system, a worst case scenario can be considered where the point of interest reside at the very edge of the pixels. For two-dimensional (2D) image this means that the sampling interval is the largest in 45 degree angle from x- and y- axis as shown in Figure 9.

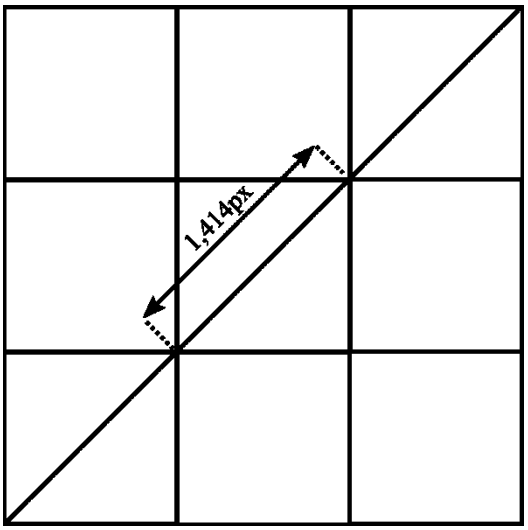

Figure 9. *A grid of pixels (3x3). The 2D sampling rate needs to be considered according to the worst-case scenario. This means that between two individual particles is an empty pixel. The longest possible route is in 45 degree angle.*

The Nyquist-Shannon sampling theorem certifies that for a sample to be completely determined from the recorded data, the sampling rate needs to be at least twice as high compared to the recorded signal. This means that the camera pixel should be at least two times smaller in one direction compared to the smallest structure to be imaged, in this case even smaller, 2,8px (2 * 1,4px) because we are in 2D image space [7]. The objective has 20x magnification and thus the pixel size of the camera should be under the maximum resolvable resolution by Rayleigh criterion multiplied by the magnification of the objective and divided by 2,8. The calculated pixel sizes compared to the maximum resolvable resolution of the objective are presented in Table 1.

Table 1. *Comparison of maximum resolvable resolution with chosen wavelength and maximum pixel size of the camera*

Laser Wavelength	488nm	561nm	638nm
Maximum Resolvable Resolution (Objective)	595nm	684nm	778nm
Maximum Pixel Size	4,25µm	4,89µm	5,47µm

The camera was chosen to be Hamamatsu Orca-Flash4.0 V2 (Hamamatsu Photonics, Hamamatsu City, Japan) digital CMOS camera based on our previous experiences. This camera has a very good resolution (2048x2048), pixel size of 6,5µm, and fast image acquisition (>100 frames/s). The theoretical resolution for the camera calculated with the values given above provides the theoretical resolution of 0,91µm. The resolution of the camera is in this case the limiting factor and we cannot capture all the information provided by the objective. Although, it is worthwhile to note that the required pixel size is calculated with the worst-case scenario and the laser wavelengths are actually not the wavelengths that are imaged. The imaged wavelengths are the emission wavelengths of the fluorophores that are used in staining the regions of interest in the imaged sample. They are always higher compared to the excitation wavelength. This means that the maximum pixel size needed for full sampling of the data is also larger.

The image acquisition speed of the camera is more than enough for our current setup. The data storing speed will be a bottleneck until different storing method is implemented. The image acquisition speed can also be raised by using binning or selecting an area of interest. This will obviously lower the resolution of the image but it will in turn make the image file size smaller. The camera also has a very low readout noise level of 1.9 electrons (r.m.s) which can be lowered even more by activating a slow scan readout mode. The slow scan mode lowers the frame rate to around 30 frames/s at full resolution but even this frame rate is good enough for our system.

Very precise motors are needed for the sample movement. In this system we have only one motorized linear stage for moving the sample along the z-axis. This is the axis that is parallel to the detection axis. The movement along the z-axis is the only linear movement that needs to be motorized for quick and precise movements. The device we used is Newport FCL100 (Newport Corporation, Irwine, United States) intelligent stepper linear stage with integrated controller. For other axes we used manual stages. We chose Standa 7T167-25 (Standa Ltd., Vilnius, Lithuania) aluminum low profile translation stages. We also used angled brackets to position all stages correctly for all three axes. As the rotational stage we chose Newport CONEX-URS50BCC (Newport Corporation, Irwine, United States) rotational stage integrated with CONEX-CC controller. This stage is used

to rotate the sample with precision. We also chose Thorlabs ST1XY-S (Thorlabs Inc., Newton, New Jersey, United States) to act as a small translation stage for aligning the center of rotation in x- and z-axis.

Illumination LED is needed for OPT back illumination and also for aligning the sample. LED can be used to align the sample without the laser turned on to minimize photobleaching. We chose a LED packed with a telecentric lens (LTCL23, Opto Engineering Srl, Mantova, Italy) to get collimated light source with a small foot print on the table.

The laser path has several optical elements: a reflective collimation gate (RC02FC-P01, Thorlabs Inc, Newton, New Jersey, USA) for the fiber (M94L01, Thorlabs Inc, Newton, New Jersey, USA), an adjustable slit (VA100C/M, Thorlabs Inc, Newton, New Jersey, USA), a cylindrical lens (ACY254-050-A, Thorlabs Inc, Newton, New Jersey, USA), two mirrors (BB1-E02, Thorlabs Inc, Newton, New Jersey, USA), two mounts for the mirrors and one for collimator (KCB1 & POLARIS-K1, Thorlabs Inc, Newton, New Jersey, USA), a telescope (AC254-050-A-ML & AC254-030-A-ML, Thorlabs Inc, Newton, New Jersey, USA), and an objective (UMPLFLN 10XW, Olympus co., Tokyo, Japan). These components are used to create the illumination light sheet. First the reflective fiber port collimates the incoming laser beam. The beam is adjusted with a mirror to travel through the optical center of the optical elements following the mirror. Next, the beam radius is increased with a telescope. It is then cropped with a slit to cut out all the light traveling outside the beam and to crop the beam before the cylindrical lens to help create thinner light sheet. The beam is then molded with a cylindrical lens to resemble a light sheet. The second mirror is set at the focal plane of the cylindrical lens so that the laser line the lens creates is thinnest. The second telescopes back focal plane is set on the mirror surface and this way the telescope will finally deliver the sheet to the illumination objective attached to the sample chamber. The telescope will also decrease the sheet to half of the original size.

The detection path consists of detection objective, filters, tube lens, and camera. Detection path works with both imaging modalities and no component changes are needed between different methods. Only filters are not going to work with every situation and can be changed or removed depending on the imaging needs. Detection objective (UMPLFLN 20XW, Olympus co., Tokyo, Japan) collects the light from the sample: fluorescent emission for SPIM and brightfield backprojection for OPT. The collected light is then run through filters. The purpose of a filter for SPIM imaging is to cut out the illumination light leaving only the emitted fluorescent light as the signal to be recorded. This means that different filters are needed to cover the different laser wavelengths and fluorescents. For OPT imaging the filter is removed altogether. It would be optimal to use motorized filter wheel to change the filter programmatically depending on the situation. However, we decided to acquire the motorized filter wheel later to keep the cost of the system down and use manual filter changing for now. After the filter the tube lens (U-TLU-1-2, Olympus co., Tokyo, Japan) focuses the detected signal to the camera. Two adapters (U-

CMAD3-1-7 & UTV1X-2-7, Olympus co., Tokyo, Japan) are installed between the camera and the tube lens to connect them. The camera was introduced earlier, but it is important to mention that the incoming light signal should cover the whole camera sensor to get the best possible resolution from the sensor.

- Objective: (UMPLFLN 20XW, Olympus co., Tokyo, Japan)
- Tube lens:
    - The lens: (U-TLU-1-2, Olympus co., Tokyo, Japan)
    - The adapters: (U-CMAD3-1-7, Olympus co., Tokyo, Japan)
    - (UTV1X-2-7, Olympus co., Tokyo, Japan)
- filter: Semrock NF03-405/488/561/635E-25 StopLine quad-notch filter

The sample chamber was designed by using the OpenSPIM-chamber as a basis. The new chamber was designed in 3D CAD design software SolidWorks (Dassault Systèmes SOLIDWORKS Corp., Waltham, Massachusetts, USA). The sample chamber will house both the detection and illumination objectives. As it will be filled with cell medium, it needs to be watertight. Objectives are immersed into the medium through the sample chamber wall. This connection is sealed with an o-ring. The chamber also needs to have an opening for the OPT illumination that is not included in the OpenSPIM-chamber. The opening was carried out in SolidWorks by removing one wall and inserting grooves to the sides that had touched this removed wall of the chamber. The grooves allowed the insertion of thin glass sheet as a wall and the glass would allow the OPT illumination to pass through. The seam between the glass and the chamber walls needs to be watertight so it is sealed with a silicone that is compatible with cells. Chamber would also need two holes for incubation fluid exchange but these can be done by drilling. The chamber floor is going to be covered by a heating element to warm the medium to the temperature suitable for living cells. The heating system is part of the incubation system. The incubation system was designed to be part of the system from the beginning, but due to problems with the main system, the incubation was left for the future. It is discussed in more detail in 5.5.

The computer used with this system is a tabletop model from Dell (Optiplex 9020, Dell Inc., Round Rock, Texas, USA). All components of the microscope are connected to the computer and are controlled by a custom control program described in chapter 3.4. The computer is fitted with Intel Core i7-4770 central processing unit (CPU) that runs at 3,40 GHz. The processor need to be able to handle the incoming data while running the control program. The camera has a minimum requirement for the processor and this requirement is met with the installed processor. The data is acquired from the camera to the computer with Active Silicon frame grabber at 100 frames per second. The computer is also retrofitted with more memory (32GB) to work as a buffer for the data coming from the camera. The data is then written to the retrofitted hard drive (4TB) that works as a work drive and temporary storage. The data is transferred from the work drive to the network drive for easy access from the computers used for the image processing.

3.3 Building the System

In the beginning the system was planned to be built on optical posts (Thorlabs Inc., Newton, New Jersey, United States). This, however, made the alignment process of the SPIM illumination path hard due to all three dimensions of movement being available. Freely movable components combined with a demand for a very accurate alignment of light sheet resulted in an unbearable problem. Every component of the illumination path of SPIM affects the creation of the light sheet and even a slight mismatch in height of the post or sideway misalignment created bad end results, the lightsheet was not of sufficient quality.

The next step in refining the system during the build included the inclusion of cage system (Thorlabs Inc., Newton, New Jersey, United States) for the components. This eliminated some of the misalignment problems but not all of them and it was not easy to try new parts in the system for the cage itself was in the way. This combined with the lingering problems with the collimation of the laser meant that even more accessible system with more stable component placement was required.

Finally, the best solution for component placement in regards to the alignment was the same dovetail rail system (Thorlabs Inc., Newton, New Jersey, United States) used in the open-SPIM project. The rail system allows the components to be moved in one dimension only. This helped the alignment process immensely. Every component is on its own rail carrier, which makes the component manipulation very easy without affecting the settings of other components.

After the component placement system was decided, it was also decided that all the optical elements should be on a small breadboard (300mm x 450mm) in case the microscope needed to be moved. The breadboard (MB3045/M, Thorlabs Inc, Newton, New Jersey, USA) was attached on top of the optical table keeping in mind to leave space for the laser and the stage stack. The laser and the stage stack are not affected by the optical height of the system, because the laser is brought to the system via optical fiber and the height of the stage stack can be adjusted. Based on this they can be situated outside of the small breadboard and leave more room for the optical component setup.

The sample chamber objective holes are fitted with o-rings to seal the medium in the chamber. After this, the sample chamber is attached to the sample chamber holder made out of aluminum. The objectives are attached to the sample chamber and sample chamber holder assembly with custom made objective holders. This way the package is sturdy and rigid. The overall assembly of sample chamber is shown in Figure 10.

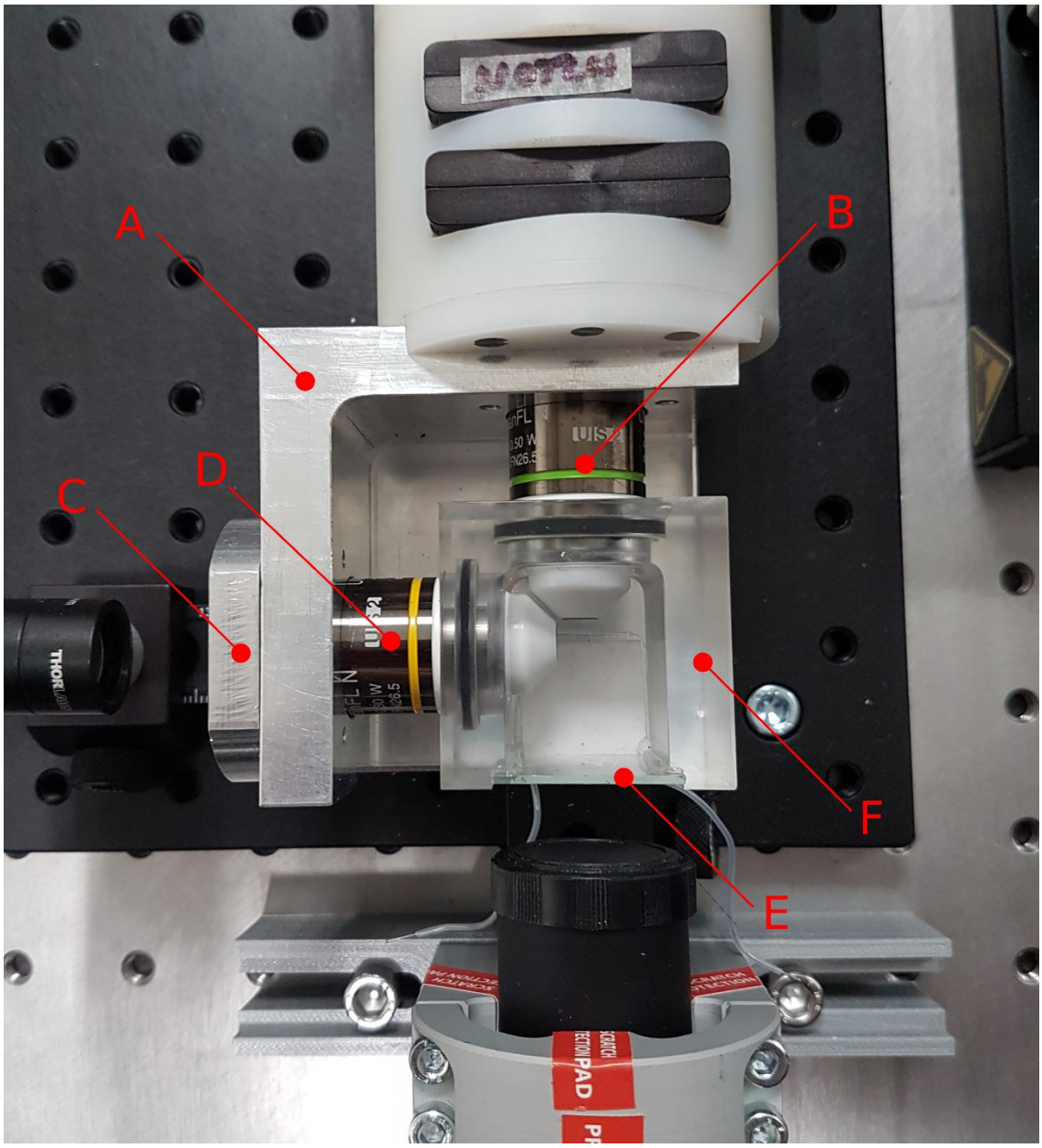

Figure 10. *Sample chamber assembly. A) Sample chamber holder, B) Detection objective, C) Objective holder ring, D) Illumination objective, E) OPT illumination window, F) Sample chamber.*

The rails are screwed on the breadboard so that the layout described in Figure 8 can be created. The sample chamber assembly is attached to a smaller rail and it defines the optical height of the system at 50mm. Raisers are designed to lift the individual components from the surface of the breadboard so that their optical axis will meet the defined height of 50mm. Raisers are designed in SolidWorks and printed with in-house 3d-printer (Ultimaker 2, Ultimaker B.V., Geldermalsen, The Netherlands).

The laser resides outside of the table to reduce the vibrations caused by the cooling fans of the laser. The laser is brought to the SPIM illumination path and the collimator with an optical fiber (M94L01, Thorlabs Inc, Newton, New Jersey, USA). The multimode fiber

has a core size of 105µm and NA of 0,11. When combined with the reflective collimator the output beam diameter is approximated to be 1,5mm by the manufacturer of the collimator although the manufacturer reminds that the multimode fiber might give worse performance compared to the single mode fiber.

3.3.1 Optical Assembly

All the single components, that are part of illumination path, were screwed to their own rail carriers with a 3D-printed piece between the component and the carrier. This combination raised the optical center of the components to the height of 50mm from the surface of the breadboard. This is the height of the optical center of illumination and detection paths dictated by the sample chamber.

The collimator and the mirrors were screwed straight to the breadboard with a 3D-printed raiser. The collimator is assembled at a 90° angle with the illumination path. The alignment mirror is attached to the end of the first illumination path rail assembly at a 45° angle so that the laser coming from the collimator is reflected to the illumination path. The collimator and the mirror are both attached to an individual mounting that provide tip and tilt plus z-axis adjustment. With these two mounts the laser can be directed accurately along the optical axis of the illumination path with the help of two alignment discs at the ends of the first rail. These discs are removed when the laser is aligned correctly.

In the end of the first rail is another mirror which reflects the light 90° towards the illumination objective in the sample chamber assembly. This mirror is also attached to an individual adjustable mounting to help with the lining of the laser sheet.

The next step was to insert the first telescope on the illumination path. The purpose of this telescope was to widen the collimated laser beam so that the y-dimension of the laser sheet would cover the field of view of the objective. The first telescope had a 3x magnification creating a beam with 4,5mm diameter. The two lenses of the telescope were set up so that the beam does not diverge or converge after the telescope.

Next, the cylindrical lens was mounted at the correct spot. The cylindrical lens focuses the light in one direction only, in this case x-axis, and leaves the other axis as is. This creates a focal line on the focal plane instead of a focal spot created by a conventional converging lens. The chosen cylindrical lens had a focal length of 50mm. This means that the correct place for the lens is 50mm from the second mirror. This creates the sharpest line on the surface of the mirror. The width of the beam can be further modified by attaching a slit on the back focal plane of the cylindrical lens. In this system an adjustable slit is used to control the beam width in x-axis. The slit takes away some of the beam intensity and by having an adjustable component the beam properties can be controlled for different imaging conditions.

The second objective is assembled between the illumination objective and the second mirror. The purpose of this telescope is to transfer the line from the mirror to the back focal plane of the mirror. The telescope also halves the dimensions of the line by using a magnification factor of 0,5x. At first the lenses are measured to the correct places but the placing can be later modified further to get a better laser sheet.

3.3.2 Mechanical Assembly

The movement stages were attached close to the sample chamber, motorized linear stage being the foundation of the stage stack. The motorized linear stage was attached to the optical table in such a way that it would move the sample through z-axis. On top of this, a manual linear stage was attached for x-axis manipulation. Another manual linear stage was attached to this with a right-angle plate for manipulating the y-axis of the sample. Another right-angle plate was attached to this with a custom-made aluminum attachment plate to accommodate the rotational stage. The rotational stage was aligned with sample chamber so that when the sample holder was set in place the end of the sample holder was in the chamber. The rotational stage was installed under the custom plate to bring it closer to the chamber to minimize vibrations through the sample holder. A two-dimensional translational optics mount for 30mm cage was used as a x-y-stage. The mount was attached to the rotational stage with two custom 3D-printed components designed with SolidWorks and printed in-house. The sample holder mechanism could then be attached on this translational stage.

The small translation stage is used to align rotational axis through the region of interest in the sample. This manual alignment step is crucial when OPT modality is being used. The back-projection algorithm used for reconstruction of OPT data will not give an accurate final result if the center of rotation is not correct. The center of rotation can be corrected further in the post processing step but getting it close to the correct position during imaging process will save time during post-processing.

At this stage the advantages of 3D-printing starts to show. The dimensions of 3D-printed pieces are not as accurate as machined pieces but for experimental use the accuracy is good enough. The ability to print complex shapes accurately very fast is invaluable at this stage. It is easy to change the design in SolidWorks and print a new piece if the previous one had some flaws. Given the nature of this work different components are tested during the build for best fit, and if some printed components need to be changed, a new one is designed and printed in its place.

3.3.3 Final Assembly

At this point the illumination LED for OPT was assembled and attached on the table just in front of the sample chamber. The assembly consisted of a raiser and the collimated

LED source with its power source. The LED is pointed at the sample chamber so that the illumination light is aligned with the detection objective.

The detection path is assembled next. It consists of the detection objective, infinity tube with filter holders, tube lens and sCMOS camera. The assembly itself is straightforward. The parts are attached to each other in the order of the aforementioned list. Only the camera is raised with a 3D-printed piece to get the center of its optical axis to 50mm. With the detection path assembled the system is ready to be tested.

3.3.4 Aligning Laser Sheet

The accurate alignment of the laser sheet is crucial to the correct functioning of the SPIM. The thinnest part of the waist of the laser light sheet needs to be in the middle of the field of view of the system. The whole sheet needs to be accurately at the focal plane of the detection objective to activate the fluorophores at the focal plane only. This creates the sectioning effect of the SPIM system.

To align the sheet with the focal plane a small calibration mirror is used at a 45° degree angle in place of normal sample to reflect the illumination light towards the camera. As the laser power of the sheet is from 1mW to 5mW, the camera needs to be protected and a neutral density (ND) filter is used to decrease the intensity. Filters with ND values of 2 and 0,6 are inserted in the detection path instead of a normal laser line multi notch filter. The laser is turned on and using the linear stages the mirror is moved to a spot where it reflects the light at the camera.

It is possible to fine tune the positions of the second telescope lenses (lenses 3 and 4), and more importantly the telescope lens 4, to make the sheet as thin as possible. By moving the latter lens it is possible to change the position of the thinnest part of the laser sheet. This needs to be positioned in the center of the field of view to maintain the sheet quality across the whole image. Because we are using the cylindrical lens instead of more intricate system, the sheet thickness changes across the image frame. If the thickness is high the sectioning capabilities of the system suffer.

The second mirror of the illumination path is then used to move the laser line to the focal plane of the camera. The focal plane is clearly shown by the line scales in the mirror, lines in the focal plane are sharp. Then, using the x-axis linear stage, the mirror is moved across the field of view to check if the laser sheet stays in focus in the whole frame. If the line is not in the focal plane the mirror is adjusted accordingly to bring the sheet to correct plane.

After the laser sheet is aligned, the ND filters are exchanged for a quad notch filter to keep the illumination laser from entering the camera. At this point the system is physically ready for imaging.

3.4 Design of the Control Program

The program to control all of the individual components of the imaging system needed to be custom built, because there was no ready control solution for the setup or for the chosen components. The control program was created in LabVIEW 2013 (National Instruments Corporation, Austin, Texas, United States) graphical programming language.

The program is going to be used by a multitude of people from different fields of expertise. Therefore, the program needs to be easy to use and comprehensible. The user interface (UI) should be clear and free of unnecessary information while providing means for controlling the imaging system without the user noticing the complexity of the software. The design of the UI should therefore be simple and divided into sections to isolate the current task from other functionality. This helps the user to get the needed data rapidly and without problems caused by the UI.

The program is designed for long data acquisition runs that can last for hours or even days. The program should therefore be as stable as possible to avoid losing data and valuable cells in the case of a malfunction. The program should be coded with robust error handling to inform the user of possible problems with the execution of the current task. Moreover, the error handling will help the administrator of the system in identifying errors in the code and fixing them.

The program should be as fast as possible in acquiring images. Fast acquisition helps the researchers in getting the information they need from the images, because the biological and physiological events can occur rapidly. It is important to capture these events for analysis. The main aim for this system is to be able to image tissue engineered samples so the speed is not the main priority, but for future application requirements its importance should not be overlooked.

In addition to the control of all the components in the system, the program takes care of the image acquisition and saving. The most important camera and laser settings should be modifiable straight from the control program to adapt the system for different samples and imaging modes. There is no need for image processing inside the control program as the processing is carried out outside the system. This means that the images can be saved directly to the hard drive. However, the preview display of the taken image is going to have some image processing options to provide more information about the image quality.

The design of the program should be as modular as possible for easy implementation of future upgrades to the system and even inclusion of the program to new microscopy systems. This was taken into consideration when designing the structure of the main program. LabVIEW is very suitable language for modular designs, because it is very easy to add functionality or modify the operation of existing programs. This is further enhanced

by LabVIEW's sub-VIs (virtual instruments). These work similarly to subroutines in other programming languages. Sub-VIs are helpful in creating a final object by combining smaller modules together.

In addition to its modularity, the program needs to be responsive to the user in case something goes wrong and the execution of the program has to be terminated during imaging. When creating responsive controls, it is imperative that the program is reacting to the user commands at all times. Under these prerequisites the main structure of the control program was chosen to be based on the producer-consumer design pattern. This structure allows the program to react to user commands even in the middle of a heavy workload.

Producer-consumer design pattern is a state machine with messaging between two loops handled by LabVIEW queue functionality. Producer loop reacts to user commands and passes them through the queue system to the consumer loop. The queue stores the commands from producer loop for the asynchronous operation of consumer loop resulting in no lost or missing commands during operation. Consumer loop is used to carry out the time-consuming operations while freeing the producer loop for user inputs. By this design the system feels responsive at all times. The structure of the main program is shown in Figure 11.

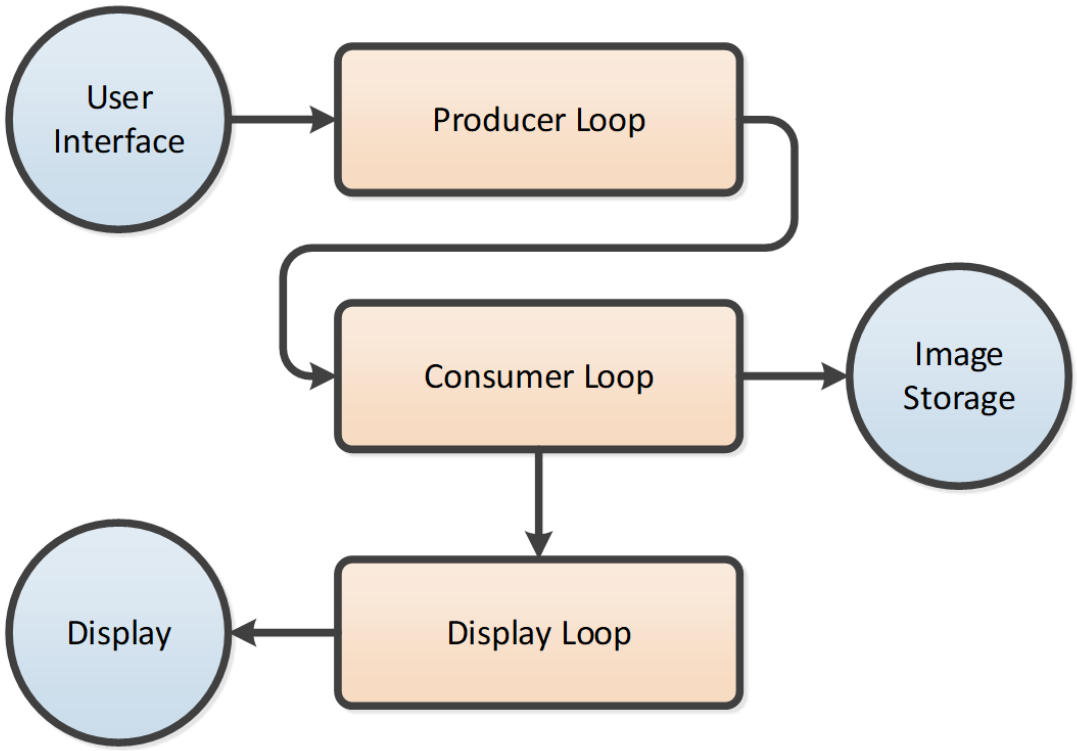

Figure 11. *The structure of the main program with producer-consumer design pattern with added display loop. Arrows show the direction of information flow.*

The imaging operations are included in the consumer loop. The consumer loop works as a state machine that is receiving the next state from the queue. It can also add a command to the queue itself and this is used to run a sequence of commands from one user input while maintaining the ability to stop the sequence by a user command. This is a very useful feature to have if the user wants to cancel unwanted operation of the system. The state machine allows the UI to be very responsive but the drawback is that it needs more time to execute compared to a straightforward imaging algorithm. This means that the image acquisition speed is lower than the optimal capability of the system. The generalized flow chart of the imaging sub-routine is presented in Figure 12.

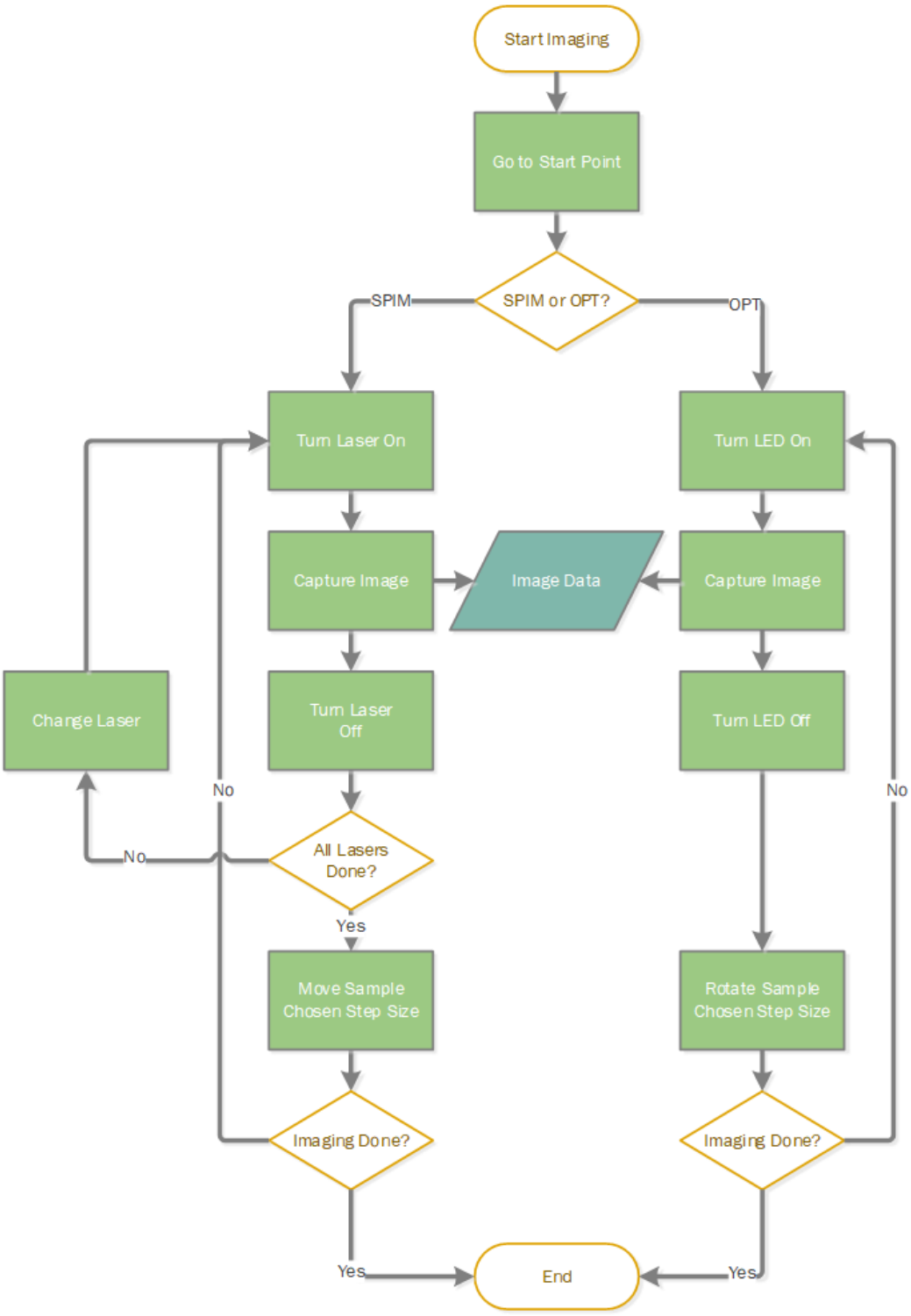

Figure 12. *The flow chart of the state machine handling the bulk of the imaging inside the consumer loop. This is highly abstracted version of the flow chart and doesn't include all of the functionality in the imaging loop. OPT and SPIM cannot be used at the same time but can be imaged one after another.*

One more loop is added to the producer-consumer design pattern to decrease the workload of the consumer loop. The added loop is called a display loop and it is used in handling all actions concerning the refreshing and updating the information output on the screen

of the computer. This includes image preview with some image processing options. The inclusion of the display loop frees the consumer loop to run the imaging process as efficiently as possible.

The image saving is carried out by an asynchronous sub-VI. The sub-VI is called from the consumer loop and it takes the image data gathered from the camera, creates a file for it and then writes the file on the hard drive. The asynchronous file saving is important for the imaging speed because if the saving is done separate from the normal operation, the consumer loop does not have to wait for the file to be saved to continue operation. This in turn makes the state machine a lot faster and the time to acquire a single frame is considerably shorter.

3.5 Cells Used for Test Images

The human adipose stem cells (hASCs) were obtained from subcutaneous adipose tissue of a female donor of 56 years in surgery at the Tampere University Hospital Department of Plastic Surgery. The procedure was carried out with the patient's written informed consent, in accordance with the Ethics Committee of the Pirkanmaa Hospital District's, Tampere, Finland, ethical approval R15161. The hASCs were isolated as reported previously [42], and expanded in Nunc T75 culture flasks (Thermo Fisher Scientific, Waltham, MA, USA) with Dulbecco's Modified Eagle Medium/Ham's Nutrient Mixture F-12 (DMEM/F-12 1:1; Thermo Fisher Scientific) supplemented with 1 % antibiotics/antimycotic containing 100 U/mL penicillin/100 U/mL streptomycin (P/S; Thermo Fisher Scientific).

Gellan gum (GG; Gelzan CM; Sigma-Aldrich, St. Louis, MO, USA) solution of 0.5% (w/v) concentration was cross-linked with bioamine spermidine trihydrochloride (SPD; BioXtra; Sigma-Aldrich) of 16% (v/v) concentration. For the fabrication of the hASC mineralization samples in hydrogel, the cells were re-suspended into GG solution heated to +37ºC, and manually mixed with the cross-linker solution to allow immediate gelation and hASC encapsulation in a 3D hydrogel.

The mineralization of hASCs was chemically induced with a previously reported osteogenic medium optimized for hASC osteogenic differentiation [42] containing DMEM/F-12 1:1 (Thermo Fisher Scientific), 5 % human serum (Biowest, Nuaillé, France), 1 % L-glutamine (GlutaMAX; Thermo Fisher Scientific), and 1% P/S and supplemented with 5 nM dexamethasone (Sigma-Aldrich), 250 µM L-ascorbic acid 2-phosphate (Sigma-Aldrich) and 10 mM β-glycerophoshate (Sigma-Aldrich).

For the hASC mineralization assay, the hASCs embedded in 3D hydrogel were stained with the OsteoImage assay according to manufacturer's protocol (Lonza, Basel, Switzerland) at 21 days. The assay was performed as a collaboration with doctoral student

Kaisa Vuornos from University of Tampere. Briefly, the cells were fixed with paraformaldehyde (Sigma-Aldrich) and the hydroxyapatite residues were stained with the OsteoImage Staining Reagent for detection at excitation/emission wavelengths (492nm/520nm).

4. RESULTS

4.1 Testing the System

In order to get an idea of how our system performs, the different properties of the system had to be tested. The speed of the system was assessed by recording multiple stacks and timing them. Furthermore, thickness of the light sheet was investigated to get an idea of the available axial resolution while imaging with the system.

4.1.1 Light Sheet Thickness

To be able to quantify the thickness of the light sheet, a measuring device is needed. The thickness is commonly measured by inserting a piece of glass on the way of the light sheet at a 45° angle [10]. The glass piece has a constant pattern or grooving on the surface with known intervals. The thickness is easily readable with this method. In this system a calibration mirror was used, although the pattern on the mirror was not used for quantification in this case, and an image stack of the light sheet was captured for analysis. One image from the stack is presented in Figure 13.

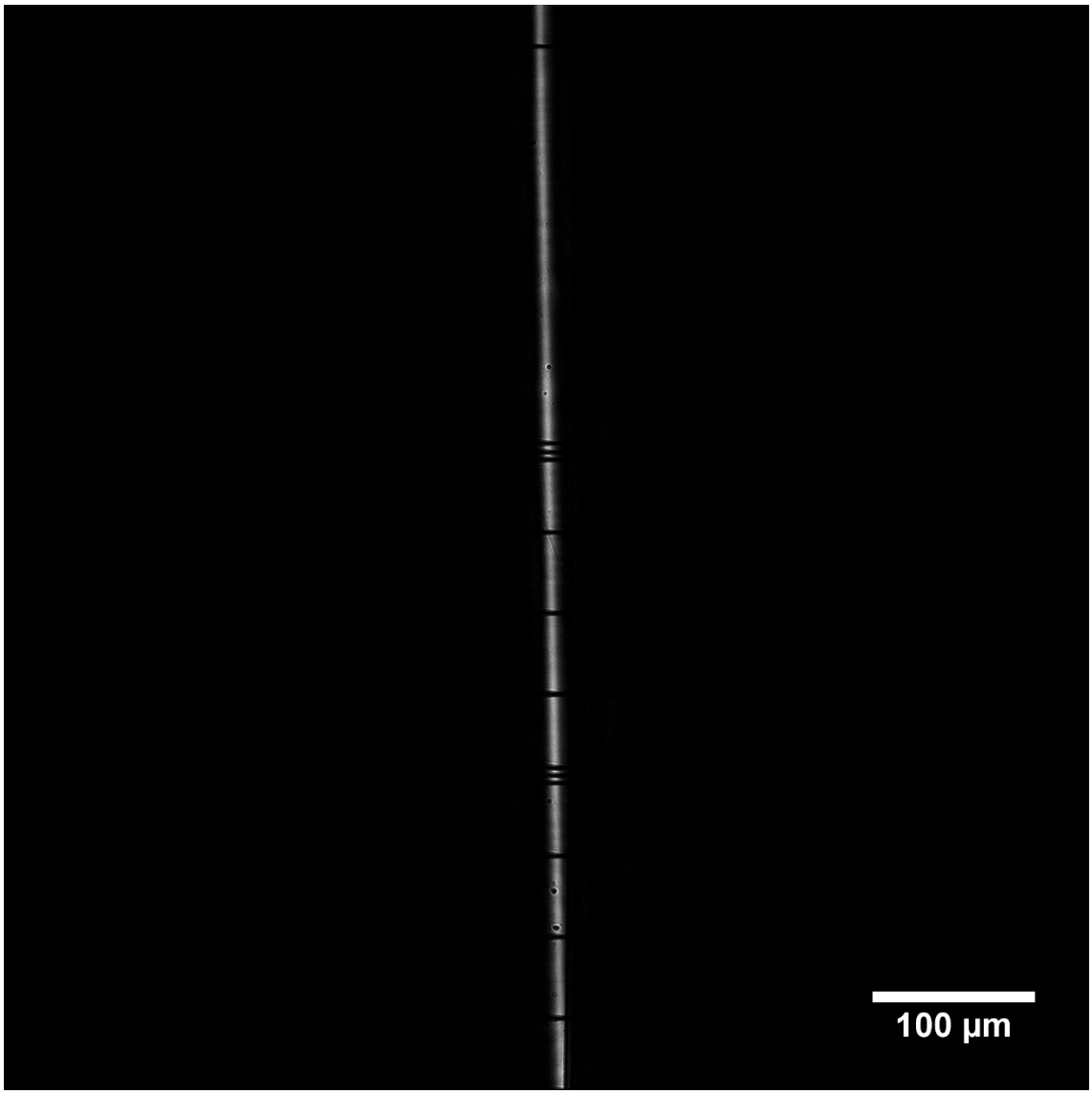

Figure 13. *The image of the light sheet when the focus is close to the middle of the calibration mirror. The grooving on the mirror is clearly visible as black horizontal lines across the laser sheet.*

The light sheet was measured in multiple focal plane positions on the mirror: middle, left and right. Due to the properties of light sheet created with cylindrical lens, the light sheet was moderately wider on the edge areas of the focal plane.

To get the light sheet thickness a full width at half maximum (FWHM) method was used. The width was analyzed from intensities of nine pixel lines in the image of the light sheet. The distribution curve of the intensities was derived in ImageJ (Ver. 1.51n, U.S. National Institute of Health, Bethesda, MD, USA) and the half intensity point was searched manually on both sides of the curve. The final light sheet thickness is the distance between these half intensity points shown in Figure 14.

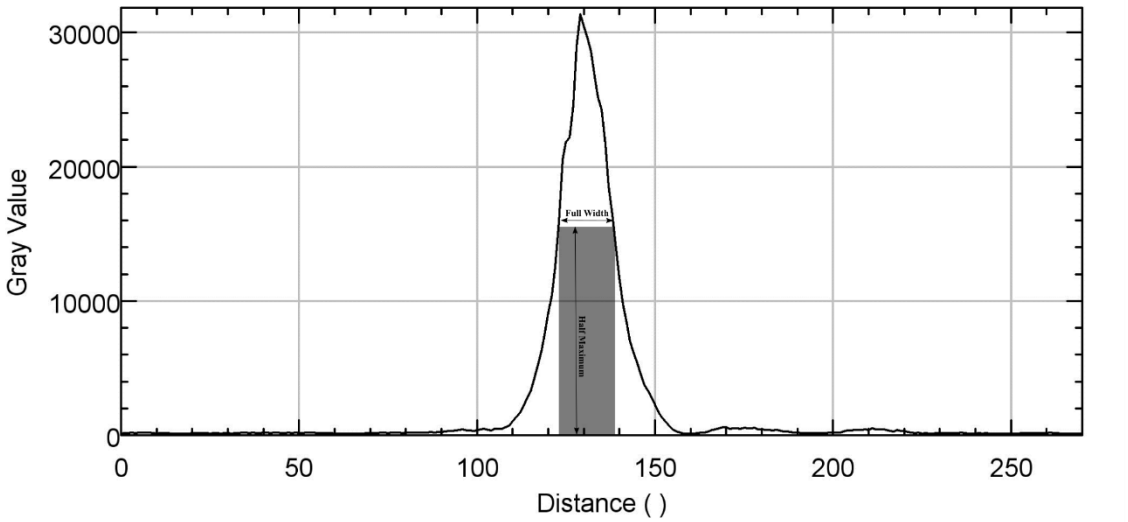

Figure 14. *Full Width Half Maximum is measured from the side profile of the light sheet. Distance is in pixels (x-axis) and Grey value is intensity (y-axis).*

The light sheet was imaged in 121 different locations as a z-stack, however all are not going to be used for the analysis of the light sheet thickness due to the manual checking of the thickness. The important locations are at the edges and the center because the differences in thickness are most prominent in these locations. Measured thicknesses can be found in Table 2.

Table 2. *Thickness of the light sheet in different part of the focal plane.*

Light Sheet Position	Left Edge of the Focal Plane	Center of the Focal Plane	Right Edge of the Focal Plane
Top of the Focal Plane	7,2µm	5,0µm	10,0µm
Middle of the Focal Plane	6,8µm	5,0µm	10,7µm
Bottom of the Focal Plane	8,8µm	5,2µm	9,7µm

4.1.2 Point Spread Function

The optical components used in the system are not ideal, for instance all the lenses and objectives. The lenses in the illumination path will cause deformations of the light sheet and the optics in detection path will cause aberrations in the captured images. The effects can be seen in the 3D diffraction pattern emitted by a point source in the sample to the camera through the detection path [43]. The shape of sub-resolution fluorescent bead

(Estapor Fluorescent Microspheres F-Y-050, Merck Chimie SAS, France), with radius of 500nm, is not round but spread. A maximum intensity projection of a single bead is presented in Figure 15. This shape deformation can be corrected with a deconvolution if the effect of the microscope to the final image is known. The point spread function (PSF) can be derived from sub-resolution bead images or a theoretical PSF can be used for deconvolution. The analysis of the PSF of this system is not included in this thesis.

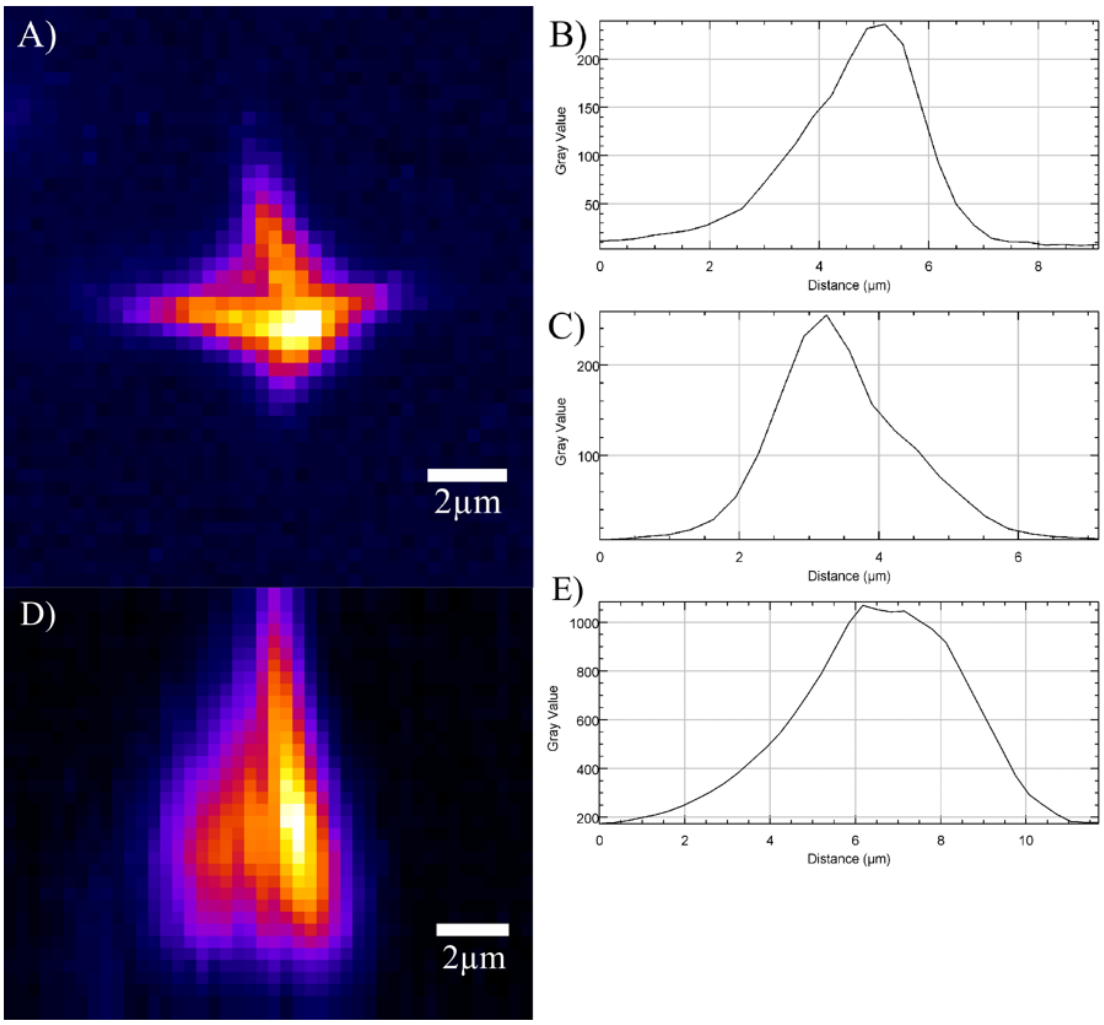

Figure 15. *A) Maximum intensity projection from xy-axis acquired from a fluorescent bead with radius of 500nm. B) Plot of intensity across x-axis. C) Plot of intensity across y-axis. D) Maximum intensity projection from yz-axis. E) Plot of intensity across z-axis*

4.1.3 Resolution of the System

Theoretical resolution of the system is reliant on the objective and the camera. As noted before in Table 1, the maximum resolvable resolution of the objective is 778nm with the wavelength of 638nm and better with shorter wavelengths.

The camera can theoretically distinguish two point sources in the distance of 910nm. This is the worst-case scenario described in 3.2.2. Usually, the resolution is calculated across one axis and the resolution for the camera is in that case 650nm and the objective is the resolution limiting factor. In both cases the theoretical value of the resolution is under 1µm. This is the case with both of the imaging modalities considering the common detection path.

4.1.4 Speed of Imaging

In order to get some estimation of the speed of the microscope, test stacks were images with both modalities and an average time was calculated from the results. In SPIM, five z-stacks of 100 slices with slice distance of 1µm were taken, while in OPT five stacks of 400 slices were taken with slice distance of 0,9° and an average time was calculated from the obtained stacks. The camera exposure time was set to 10ms for both imaging methods. The results of the speed test are shown in Table 3. They are not comparable to any other microscope as such but they will regardless give a rough indication on how long it takes to image a sample with the developed system.

Table 3. *Imaging time averaging for both modalities. Imaging time will vary according to the used exposure time.*

Modality	OPT (400 images)	SPIM (100 images)
Test Stack 1	320s	74s
Test Stack 2	320s	75s
Test Stack 3	319s	74s
Test Stack 4	320s	75s
Test Stack 5	319s	75s
Average time of test stacks	320s	75s
Average time for single frame	0,80s	0,75s
Single frame without exposure time (10ms)	0,70s	0,65s

4.2 Control Program

The control program is very stable and responsive to user commands as intended. The error checking inside the program is very robust and the administrator of the system receives accurate information on the problems. The UI is clear and easy to use. The program is modular and the chosen producer-consumer setup for the main structure is reliable. Front page of the UI can be seen in Figure 16.

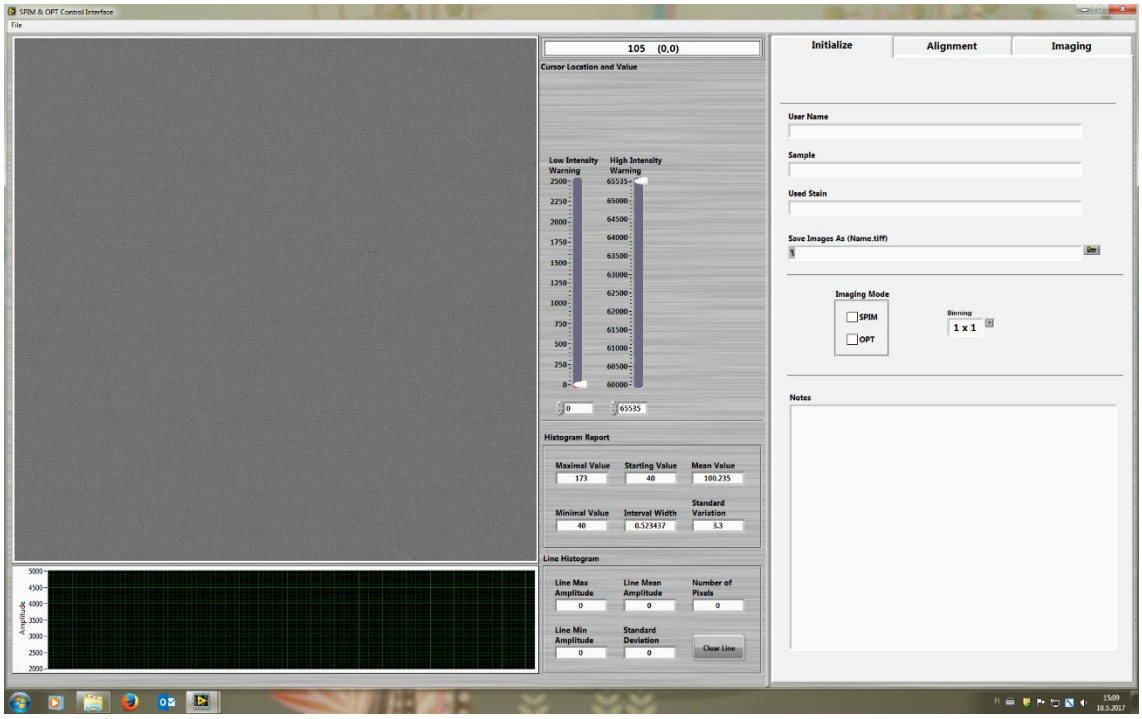

Figure 16. *Front page of the microscopy program. The UI is clear and most of the functionality is hidden under several tabs. This way the user only sees a specific set of information at the time. (Left) The preview image takes most of the screen with the histogram information. (Right) User tabs take one third of the screen area. Different functionality can be accessed through the tabs shown at the top right.*

4.3 Images

The images shown here are human adipose stem cells described earlier in 3.5. The cells are clearly visible in the bright-field images (Figure 17.) but the mineralization nodules are hard to distinguish without referring to the fluorescence images (Figure 18.). The nodules can be identified in the fluorescence images with ease. Hydrogel structures can be observed in the bright-field image. The reconstruction of a SPIM z-stack is presented in Figure 19.

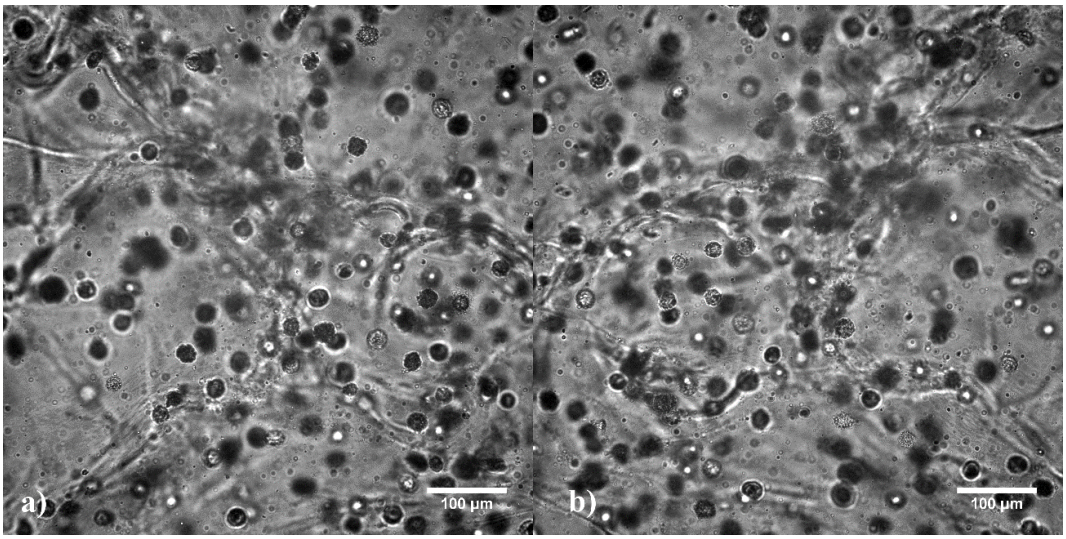

Figure 17. *Two bright-field images taken from a sample containing human adipose stem cells with different angular positions. Focal plane is set to the center of the sample tube. a) Rotation of 162 degrees. b) Rotation of 351 degrees.*

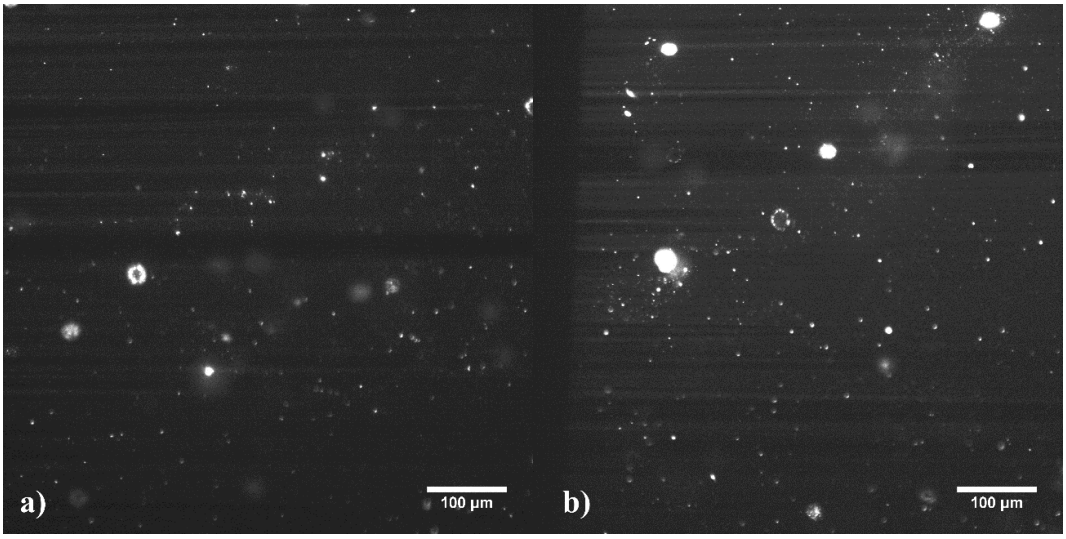

Figure 18. *Two fluorescence images taken from different depths in the sample containing human adipose stem cells. Images have been post-processed to show the streaking effect inherent to SPIM. Original images are not overexposed. a) Image from a depth of 447µm. b) Image from a depth of 804µm. Excitation 480nm, emission 520nm.*

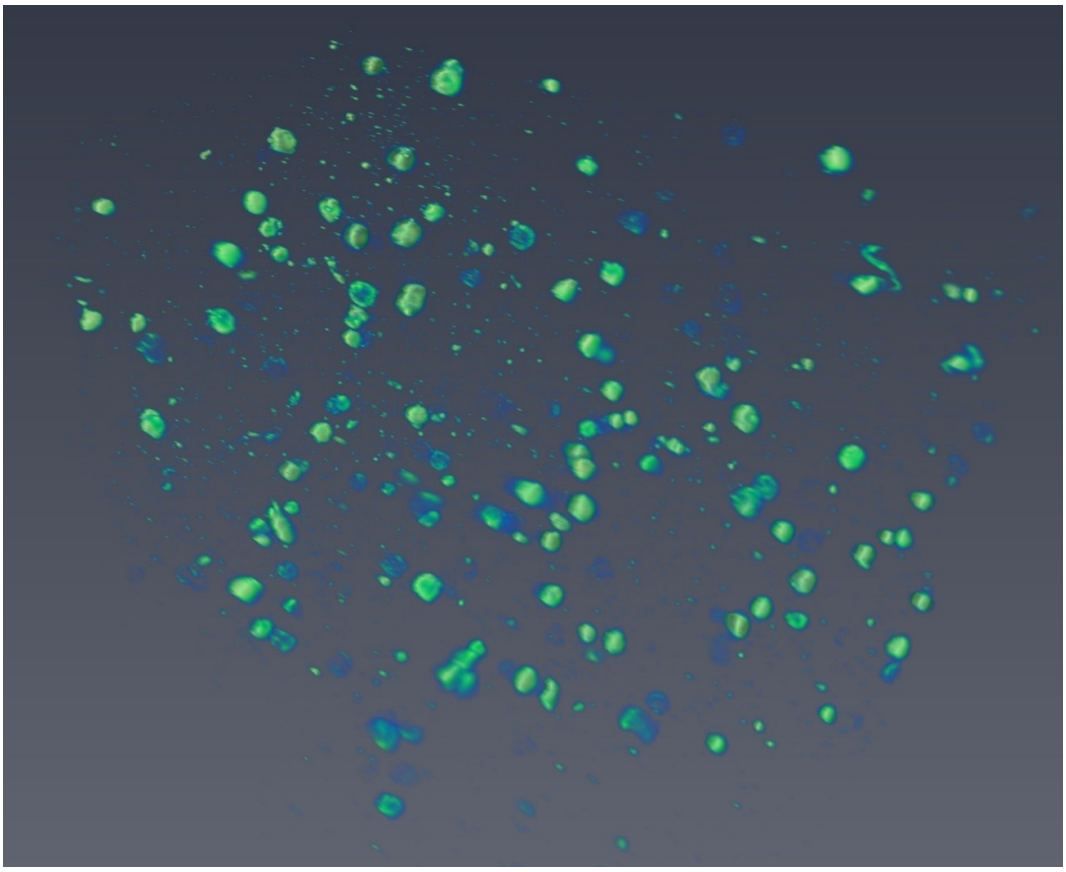

Figure 19. *3D reconstruction of the SPIM stack with the human adipose stem cells. The different cells are easily defined and the small granules of mineralization are also clearly visible.*

5. DISCUSSION

5.1 System Overview

The optical 3D-imaging system developed during this thesis is an upgrade of the OpenSPIM-system. It is capable of imaging non-opaque samples up to 1mm thick. The system also includes OPT for brightfield 3D imaging needs.

Some of the functionality originally planned were omitted during the development process due to challenges in the design but the main features needed for the multimodal imaging were successfully established.

5.2 Properties of the System

The main feature of the system is the inclusion of both OPT and SPIM. The built system is capable of capturing high resolution (SPIM: lateral <1µm, axial < 6µm, OPT: spatial <1µm) images of TE products in hydrogel scaffolds with both modalities.

The SPIM part is an obvious upgrade on the OpenSPIM-system with three available laser lines. This enables biologists to have more options when choosing fluorophores for their samples. With three different wavelengths at their disposal, different structures in the sample can be simultaneously stained with separate fluorophores to obtain more information from the cell structures and functionality.

The inclusion of OPT is the most prominent alteration when compared to the OpenSPIM-system. The addition of illumination for OPT is not the only feature required for the operational OPT system. The rotational motor has to be very accurate because the OPT relies on the rotation of the sample to obtain accurate reconstructions.

Resolution of the system is exceedingly difficult to calculate accurately without comprehensive tests. The camera appeared to be the limiting factor, although the calculations used in this thesis considered the most unfavorable or “unfortunate” situation. Using the calculations regularly used the camera can detect smaller detail and the objective becomes the limiting factor. In the real system, the resolution will be worse compared to calculations due to imperfections in the detection components, for instance aberrations in the detection objective.

On the other hand, to have precise information regarding the axial resolution, it was important to have accurate value for the light sheet thickness. The lower the value of the light sheet thickness is, the better is the axial resolution. Even the depth of focal plane of the objective does not affect the improved resolution because the fluorescent signal is

emitted from a very confined area activated by the laser sheet. The alignment problems of the initial laser beam or optical components in the illumination path will have a deteriorating effect on the quality of the light sheet.

As seen on Table 2, the light sheet gets thicker when getting closer to the edges of the field of view (FOV). On the left side the sheet is relatively close to the center thickness but on the right edge it gets reasonably wider. This can be caused by the scattering in the immersion liquid (water) or by illumination axis component placement. These differences are not considerable as the right side of the image regardless suffers from degradation of the light sheet during the imaging. This reduction in image quality can be prevented by imaging the sample from different directions and stitching the final stack together from multiple stacks. This is the norm when imaging highly scattering samples, for instance tissue samples which are the main targets for this system in addition to cells immersed in hydrogel scaffolds.

Taken together, the light sheet thickness is very good considering the system and gives the axial resolution necessary to image the samples the system is designed for. The light sheet thickness is comparable to the publications and resources on SPIM [10][44][41]. The illumination path can be modified later if a need arises to get better axial resolution.

It is possible to clearly see individual cells and cell structures from the captured images. The cell shape and even some structures of the cells can be detected with different fluorescent dyes. The cells are clearly visible in our test images shown in Figure 17 and in addition to cells, small mineralization nodules can be identified in Figure 18. This shows that the system can be used to gather complementary data from the sample. The mineralization shown in the bright-field images and the fluorescence images can be used to help identify single nodules from the hydrogel structures. The system has adequate resolution to get the necessary data to develop the TE products it was designed to image.

In addition to the point spread function, the speed of the system can be very difficult to measure. OPT and SPIM both rely on different methods to create the image and the imaging time depends heavily on the exposure time of the camera. Usually the exposure time for fluorescence imaging is higher because the intensity of the fluorescence is lower when compared to the straightforward bright-field illumination of OPT. This in turn means that the exposure time of the camera needs to be higher to get sufficient dynamic range in the image. Other factors taking time during the imaging is the movement of the rotational and/or linear stages between slices, however this depends heavily on the moved distance.

The results show that imaging time difference between test stacks is only one second at maximum. The time difference for single frames is minor between modalities. Imaging system is thus capable of capturing an image every second even with higher exposure times and most of the time is spent moving the sample. The time to adjust the sample can

be calculated from the averaged slices by deducting the exposure time from the average time for single frame.

5.3 Usability

The usability of the program is subjective and entails a lot of testing with different users to be optimized. The focus was to finish the initial imaging rapidly with minimal time spent for the unnecessary option. Imaging with the system is intuitive and easy.

With most of the functionality divided to separate tabs according to their function, only the required information for the task at hand is visible. The buttons are large and easily identifiable for effortless manipulation. Color coding was used with buttons to identify the various different functions they have, while some of the buttons have been coded to change color when pressed to inform the user. This helps with the information flow from the control program to the user.

The simplicity of the controls is possible because the system is highly specialized for a specific sample type. The custom control program eliminates the need for multitude of myriad controls that would be necessary if the program was universal for different configurations of parts. Therefore, the usability of the program remains clear and intuitive.

Despite the user-friendly controls, the usability of the physical microscopy system is not as good as the program. Due to problem with collimating several laser wavelengths at the same time, the laser line needs to be chosen manually. In fact, this was shown to improve the safety of the system, because it is impossible to find laser safety glasses that protect the eyes from all available wavelengths while imaging. The system is not sealed and therefore the laser can leak and reflect from the illumination path if used carelessly. Because the laser is chosen manually, the user is able to change the correct protective glasses between imaging runs.

In addition to the laser line, the filters need to be changed manually and all linear stages, except the z-stage, are moved by hand. This can be a source of error and it will take extra time to prepare the sample for imaging if the user is not familiar with the system. The hardware is positioned to make the manual operations as convenient as possible but this can still be a hindrance.

5.4 Challenges During Development

The development of the system was challenging and a lot of the desired functionality remains under construction. To date, only the basic core of the imaging system has been built mainly due to the problems with the laser illumination and manufacturing of the custom parts.

Firstly, the laser we had ordered was to output polarized laser. This proved to be essentially impossible to manufacture with the given specifications and the blue wavelength (488nm) laser was very unstable. Despite the efforts of the manufacturer, the laser was delivered very late from the original delivery date and yet the blue laser was not working properly. The laser was not able to output over 5mW and could turn off without warning even at lower power. Therefore, it could stop working in the middle of imaging.

Secondly, the laser illumination had five different wavelengths from two different lasers to be collimated with one fiber port. Ultimately, this was a very difficult problem to solve. The lasers had different number of output configurations: one had three while the other had just one output port. Combining these beams in one fiber was very difficult with the available resources. Multiple collimators were tested and none of them gave adequate results. Finally, it was decided to only use one laser system with three different wavelengths. The chosen laser had wavelengths our researchers were most interested in (488nm, 561nm and 638nm).

The laser we decided to use has three individual outputs and the best way to import this to the illumination path includes three different collimators and dichroic mirrors to combine the collimated beams. Finally, we decided to use a single collimator and choose the laser line manually. This makes the imaging slower but saved us resources for further development.

Lastly, most of the metal and plastic parts for the microscope needed to be custom-made and this delayed the project for months. The task of manufacturing the parts were assigned to the workshop of the Tampere University of Technology. The hierarchy structure of the University has been under change during the thesis and unfortunately our parts got lost in the process which caused additional delay. Furthermore, some of the parts were ordered from abroad and a lot of bureaucracy was required to get the parts to Finland. Overall, the manufacturing process suffered from a lack of information flow and this caused an unnecessary halt in designing the system.

5.5 Future Upgrades to the System

The basic multimodal SPIM/OPT is a very good starting point for further development. The system is highly modular and every component is changeable. The program is designed to be easily modified according to the needs of the user while still being simple and intuitive to use. These factors make any plausible upgrades easy to implement.

The main upgrade for the system in the future is the incubation system. The sample chamber is already fitted with a heating element and most of the parts for the gas exchange have been acquired. The final implementation of the incubator was omitted from this work due to the amount of labor it requires. The incubator allows time lapse imaging by providing nutrients and gas exchange for the imaged sample. One of the problems with

the incubation is the open topped sample chamber and the gas exchange method needs to be carefully designed.

Another upgrade for the system could be motorization of the manual linear stages, motorized filter wheel and better laser line choosing mechanism. This upgrade doesn't affect the system functionality as such. While the UI of the program will have more buttons and additions to the hardware will increase its complexity, most of the novel functionality can be hidden under the current functionality. This way the UI of the control program will still have a simple and clean look but the functionality of the system will be improved significantly.

The image quality will be increased with the implementation of a point spread function derived deconvolution. This will reduce blurring of the image and thus, increase the perceived resolution. Image features will become a lot sharper and more information on the imaged sample will be revealed. Commercial imaging software suites will be tested in the future for handling the deconvolution.

In order to get rid of the artefacts in the fluorescence images, an upgrade to the illumination part of SPIM is required. To improve the image quality, it is essential to reduce the inherent problems typical to the SPIM systems, such as streaking and laser sheet deterioration on the far side of the sample. The upgrade would include another illumination path from the opposite side of the current illumination path and galvanometric mirrors to insert the light sheet in the sample chamber from different angles and directions. These modifications would help to reduce the streaking.

Imaging speed upgrade can also become necessary if a fast imaging is required for future samples. This upgrade would be entirely program based because the camera was chosen to have very fast image acquisition rate. The speed of the system depends on the achieved dynamic range with fast exposure times and its limit can probably be identified.

If the speed of the system is increased, the infrastructure has to be upgraded accordingly. The amount of stored data will increase dramatically as the camera output can get up to 800MB/s. Typical hard drives cannot handle this kind of data stream and four solid-state drives (SSD) are required in a redundant array of independent disc (RAID) setting to save all the data straight to disc.

6. CONCLUSIONS

The aim of this thesis was to build a multimodal imaging system combining OPT and SPIM with custom control program. The main focus was to create a system capable of imaging TE samples with high resolution while offering environmental controls to keep the sample alive for several days. The constructed system was tested for technical quality with real hydrogel and cell samples to assess its capability to image TE constructs.

The system performs as planned and it has been used for imaging samples embedded in hydrogel. The resolution of the system is very good and analysis of TE samples is possible. Compared to the OpenSPIM system, this built system is a clear upgrade featuring full OPT functionality and multiple laser lines to choose from. The features included in the system open up new possibilities in the field of TE research.

Most of the required features have been implemented during this thesis. The incubation system is the most notable assembly missing from the system. It is required for more time-consuming imaging runs to sustain the vital functions of the imaged sample. Therefore, it will be included to the system in the near future to improve the imaging capabilities.

In conclusion, the system is functional and it will be used for hydrogel and TE-sample imaging. Furthermore, the system works as a basis for future studies in enhancing the imaging of TE-products.

REFERENCES

[1] A. A. Appel, M. A. Anastasio, J. C. Larson, and E. M. Brey, "Imaging challenges in biomaterials and tissue engineering," *Biomaterials*, vol. 34, no. 28, pp. 6615–6630, 2013.

[2] E. Figueiras, A. M. Soto, D. Jesus, M. Lehti, J. Koivisto, J. E. Parraga, J. Silva-Correia, J. M. Oliveira, R. L. Reis, M. Kellomäki, and J. Hyttinen, "Optical projection tomography as a tool for 3D imaging of hydrogels.," *Biomed. Opt. Express*, vol. 5, no. 10, pp. 3443–9, 2014.

[3] T. Vo-dinh, "Biomedical Photonics," p. 1787, 2003.

[4] "Molecular Expressions Microscopy Primer: Anatomy of the Microscope." [Online]. Available: http://micro.magnet.fsu.edu/primer/anatomy/anatomy.html. [Accessed: 14-May-2017].

[5] J. Huisken and D. Y. R. Stainier, "Selective plane illumination microscopy techniques in developmental biology.," *Development*, vol. 136, no. 12, pp. 1963–1975, 2009.

[6] "Optical Imaging | National Institute of Biomedical Imaging and Bioengineering." [Online]. Available: http://www.nibib.nih.gov/science-education/science-topics/optical-imaging. [Accessed: 17-Sep-2016].

[7] J. Pawley and J. B. Pawley, "Handbook Of Biological Confocal Microscopy," *Handb. Biol. Confocal Microsc.*, no. August, p. 985, 2006.

[8] J. Sharpe, U. Ahlgren, P. Perry, B. Hill, A. Ross, J. Hecksher-Sørensen, R. Baldock, and D. Davidson, "Optical projection tomography as a tool for 3D microscopy and gene expression studies.," *Science*, vol. 296, no. 2002, pp. 541–545, 2002.

[9] D. Huang, E. A. Swanson, C. P. Lin, J. S. Schuman, W. G. Stinson, W. Chang, M. R. Hee, T. Flotte, K. Gregory, C. A. Puliafito, and J. G. Fujimoto, "Optical Coherence Tomography HHS Public Access," *Sci. Novemb.*, vol. 22, no. 2545035, pp. 1178–1181, 1991.

[10] J. Huisken, J. Swoger, F. Del Bene, J. Wittbrodt, and E. H. K. Stelzer, "Optical sectioning deep inside live embryos by selective plane illumination microscopy.," *Science*, vol. 305, no. August, pp. 1007–1009, 2004.

[11] T. Planchon, "Light Sheet Imaging for Fast 3D Live Cell and Tissue Imaging." [Online]. Available: http://www.leica-microsystems.com/science-lab/webinar-light-sheet-imaging-for-fast-3d-live-cell-and-tissue-imaging/. [Accessed: 18-May-2017].

[12] "Molecular Expressions Microscopy Primer: Specialized Microscopy Techniques - Fluorescence Microscopy." [Online]. Available: http://micro.magnet.fsu.edu/primer/techniques/fluorescence/fluorhome.html. [Accessed: 14-Jul-2015].

[13] Nobelprize.org, "The Nobel Prize in Chemistry," *The Nobel Prize in Chemistry 2014*, 2014. [Online]. Available:

http://www.nobelprize.org/nobel_prizes/chemistry/laureates/2014/. [Accessed: 29-May-2015].

[14] D. C. Prasher, V. K. Eckenrode, W. W. Ward, F. G. Prendergast, and M. J. Cormier, "Primary structure of the Aequorea victoria green-fluorescent protein," *Gene*, vol. 111, no. 2, pp. 229–233, Feb. 1992.

[15] "Nikon MicroscopyU | Fluorescence Microscopy | Introduction." [Online]. Available: http://www.microscopyu.com/articles/fluorescence/fluorescenceintro.html. [Accessed: 14-Jul-2015].

[16] J. W. Dobrucki, D. Feret, and A. Noatynska, "Scattering of exciting light by live cells in fluorescence confocal imaging: phototoxic effects and relevance for FRAP studies.," *Biophys. J.*, vol. 93, no. 5, pp. 1778–1786, 2007.

[17] R. Dixit and R. Cyr, "Cell damage and reactive oxygen species production induced by fluorescence microscopy: effect on mitosis and guidelines for non-invasive fluorescence microscopy.," *Plant J.*, vol. 36, no. 2, pp. 280–290, 2003.

[18] W. J. Smith, *Modern Optical Engineering*. 2000.

[19] "Method of the Year 2014," *Nat. Methods*, vol. 12, no. 1, pp. 1–1, 2014.

[20] H. Siedentopf and R. Zsigmondy, "Uber Sichtbarmachung und Größenbestimmung ultramikoskopischer Teilchen, mit besonderer Anwendung auf Goldrubingläser," *Ann. Phys.*, vol. 315, no. 1, pp. 1–39, 1902.

[21] A. H. Voie, D. H. Burns, and F. A. Spelman, "Orthogonal-plane fluorescence optical sectioning: Three-dimensional imaging of macroscopic biological specimens," *J. Microsc.*, vol. 170, no. 3, pp. 229–236, 1993.

[22] M. Weber, M. Mickoleit, and J. Huisken, *Light sheet microscopy*, 1st ed., vol. 123. Elsevier Inc., 2014.

[23] J. Huisken and D. Y. R. Stainier, "Even fluorescence excitation by multidirectional selective plane illumination microscopy (mSPIM).," *Opt. Lett.*, vol. 32, no. 17, pp. 2608–2610, 2007.

[24] a. Kaufmann, M. Mickoleit, M. Weber, and J. Huisken, "Multilayer mounting enables long-term imaging of zebrafish development in a light sheet microscope," *Development*, vol. 139, pp. 3242–3247, 2012.

[25] a. Bassi, B. Schmid, and J. Huisken, "Optical tomography complements light sheet microscopy for in toto imaging of zebrafish development," *Development*, pp. 1016–1020, 2015.

[26] K. Greger, J. Swoger, and E. H. K. Stelzer, "Basic building units and properties of a fluorescence single plane illumination microscope," *Rev. Sci. Instrum.*, vol. 78, 2007.

[27] C. J. Engelbrecht and E. H. Stelzer, "Resolution enhancement in a light-sheet-based microscope (SPIM).," *Opt. Lett.*, vol. 31, no. 10, pp. 1477–1479, 2006.

[28] H. Corporation, "ORCA-Flash4.0," 2012.

[29] W. Denk, J. H. Strickler, and W. W. Webb, "Two-photon laser scanning fluorescence microscopy.," *Science*, vol. 248, no. 4951, pp. 73–6, 1990.

[30] P. T. C. So, “Two-photon Fluorescence Light Microscopy,” pp. 1–5, 2002.

[31] M. Mickoleit, B. Schmid, M. Weber, F. O. Fahrbach, S. Hombach, S. Reischauer, and J. Huisken, “High-resolution reconstruction of the beating zebrafish heart.,” *Nat. Methods*, no. July, pp. 1–6, 2014.

[32] B. Schmid, G. Shah, N. Scherf, M. Weber, K. Thierbach, C. P. Campos, I. Roeder, P. Aanstad, and J. Huisken, “High-speed panoramic light-sheet microscopy reveals global endodermal cell dynamics.,” *Nat. Commun.*, vol. 4, p. 2207, 2013.

[33] U. Krzic, S. Gunther, T. E. Saunders, S. J. Streichan, and L. Hufnagel, “Multiview light-sheet microscope for rapid in toto imaging,” *Nature Methods*, vol. 9. pp. 730–733, 2012.

[34] J. Swoger, P. Verveer, K. Greger, J. Huisken, and E. H. K. Stelzer, “Multi-view image fusion improves resolution in three-dimensional microscopy.,” *Opt. Express*, vol. 15, no. 13, pp. 8029–8042, 2007.

[35] J. Sharpe, “Optical projection tomography as a new tool for studying embryo anatomy,” *J. Anat.*, vol. 202, pp. 175–181, 2003.

[36] J. R. Walls, J. G. Sled, J. Sharpe, and R. M. Henkelman, “Resolution improvement in emission optical projection tomography.,” *Phys. Med. Biol.*, vol. 52, pp. 2775–2790, 2007.

[37] A. Bassi, L. Fieramonti, C. D’Andrea, M. Mione, and G. Valentini, “In vivo label-free three-dimensional imaging of zebrafish vasculature with optical projection tomography,” *J. Biomed. Opt.*, vol. 16, p. 100502, 2011.

[38] A. Arranz, D. Dong, S. Zhu, M. Rudin, C. Tsatsanis, J. Tian, and J. Ripoll, “Helical optical projection tomography.,” *Opt. Express*, vol. 21, no. 22, pp. 25912–25, 2013.

[39] J. R. Walls, J. G. Sled, J. Sharpe, and R. M. Henkelman, “Correction of artefacts in optical projection tomography.,” *Phys. Med. Biol.*, vol. 50, pp. 4645–4665, 2005.

[40] J. Mayer, A. Robert-Moreno, R. Danuser, J. V Stein, J. Sharpe, and J. Swoger, “OPTiSPIM: integrating optical projection tomography in light sheet microscopy extends specimen characterization to nonfluorescent contrasts.,” *Opt. Lett.*, vol. 39, no. 4, pp. 1053–6, 2014.

[41] “OpenSPIM.” [Online]. Available: http://openspim.org. [Accessed: 09-May-2016].

[42] L. Kyllonen, S. Haimi, B. Mannerstrom, H. Huhtala, K. M. Rajala, H. Skottman, G. K. Sandor, and S. Miettinen, “Effects of different serum conditions on osteogenic differentiation of human adipose stem cells in vitro,” *Stem Cell Res Ther*, vol. 4, no. 1, p. 17, 2013.

[43] C. Zeiss and M. Online, “Carl Zeiss Microscopy Online Campus The Point Spread Function,” 2016. [Online]. Available: http://zeiss-campus.magnet.fsu.edu/articles/basics/psf.html. [Accessed: 24-Aug-2015].

[44] E. J. Gualda, T. Vale, P. Almada, J. A. Feijo, G. G. Martins, and N. Moreno, “OpenSpinMicroscopy: an open-source integrated microscopy platform,” *Nat*

Meth, vol. 10, no. 7, pp. 599–600, Jul. 2013.

APPENDIX 1: MAIN PROGRAM

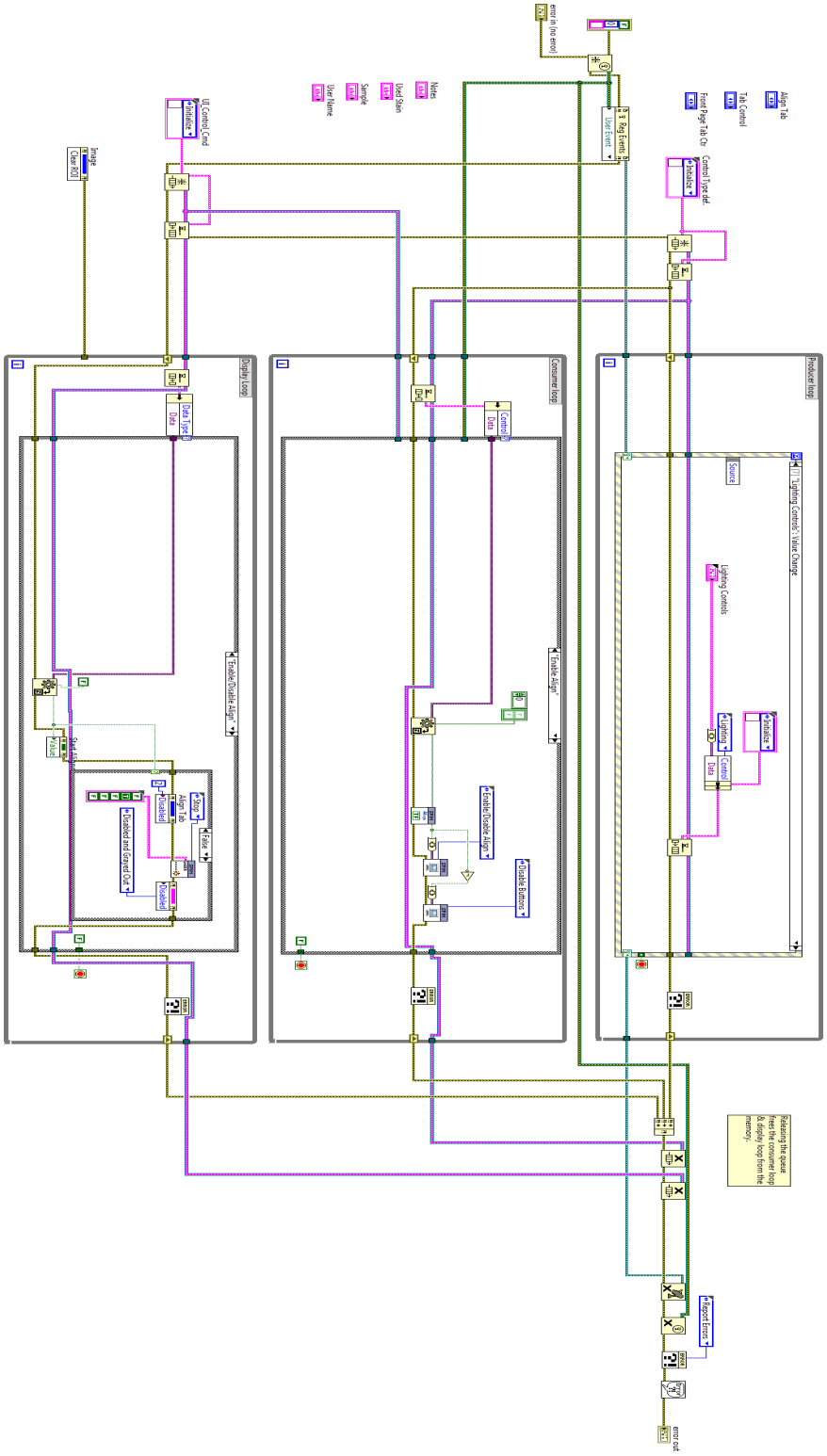

Figure 20. *The structure of the main program*

APPENDIX 2: IMAGE SUBROUTINE

Figure 21. *Image-subroutine control panel*

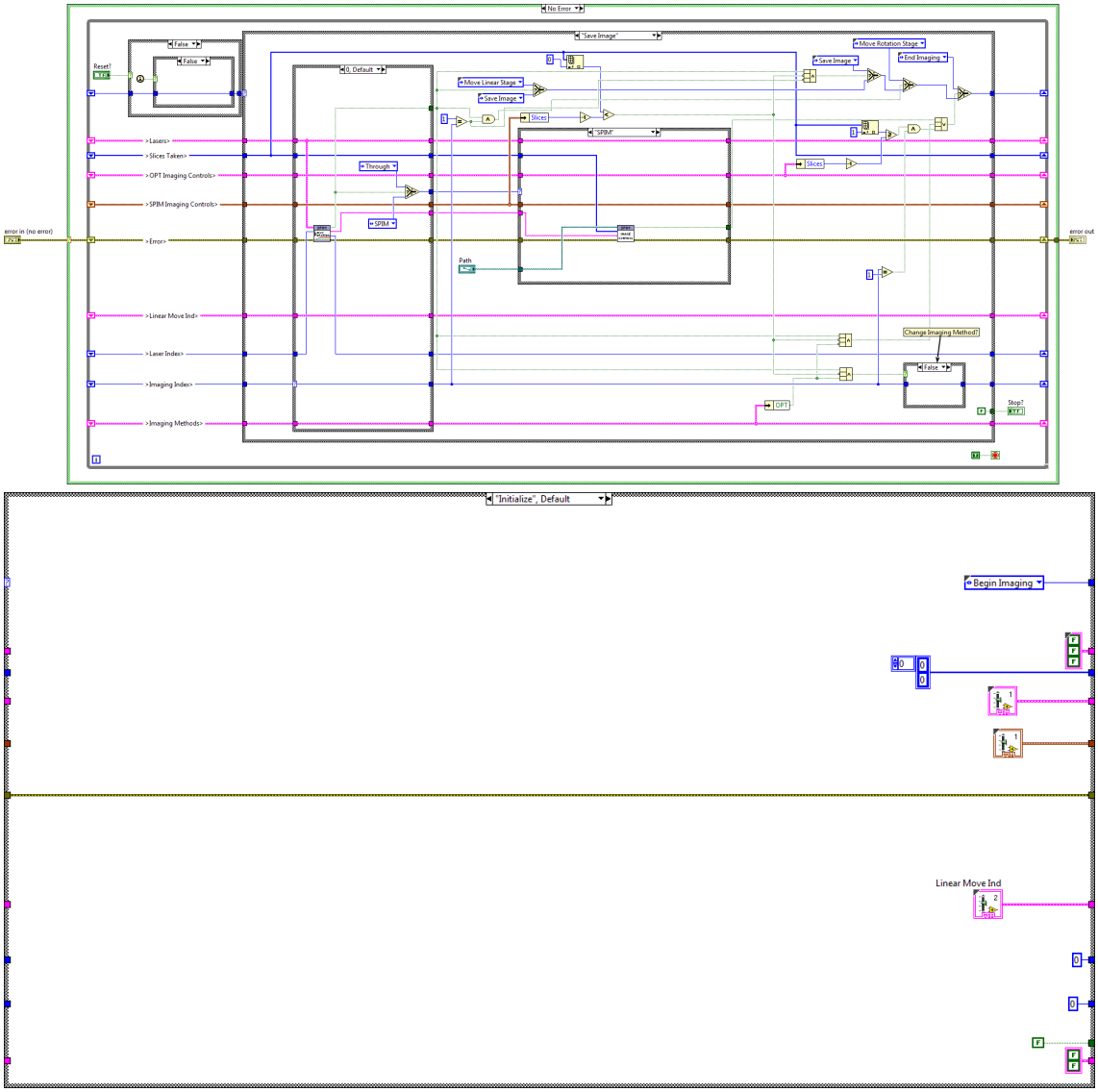

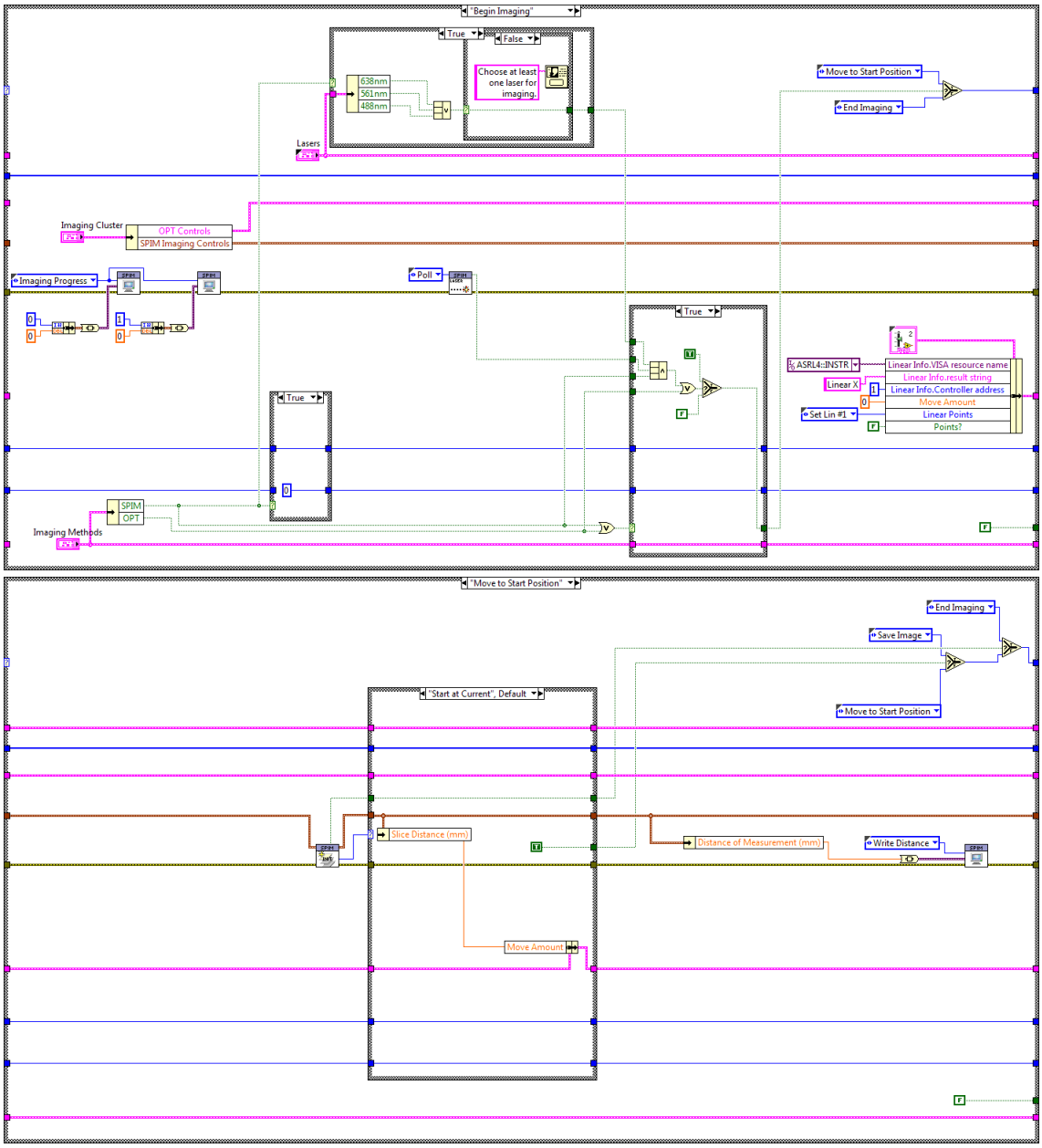
"Begin Imaging"
True
False
638nm
561nm
488nm
Choose at least one laser for imaging.
Lasers
Move to Start Position
End Imaging
Imaging Cluster
OPT Controls
SPIM Imaging Controls
Imaging Progress
Poll
True
ASRL4::INSTR
Linear Info.VISA resource name
Linear Info.result string
Linear X
Linear Info.Controller address
Move Amount
Set Lin #1
Linear Points
Points?
True
SPIM
OPT
Imaging Methods
"Move to Start Position"
End Imaging
Save Image
Move to Start Position
"Start at Current", Default
Slice Distance (mm)
Distance of Measurement (mm)
Write Distance
Move Amount

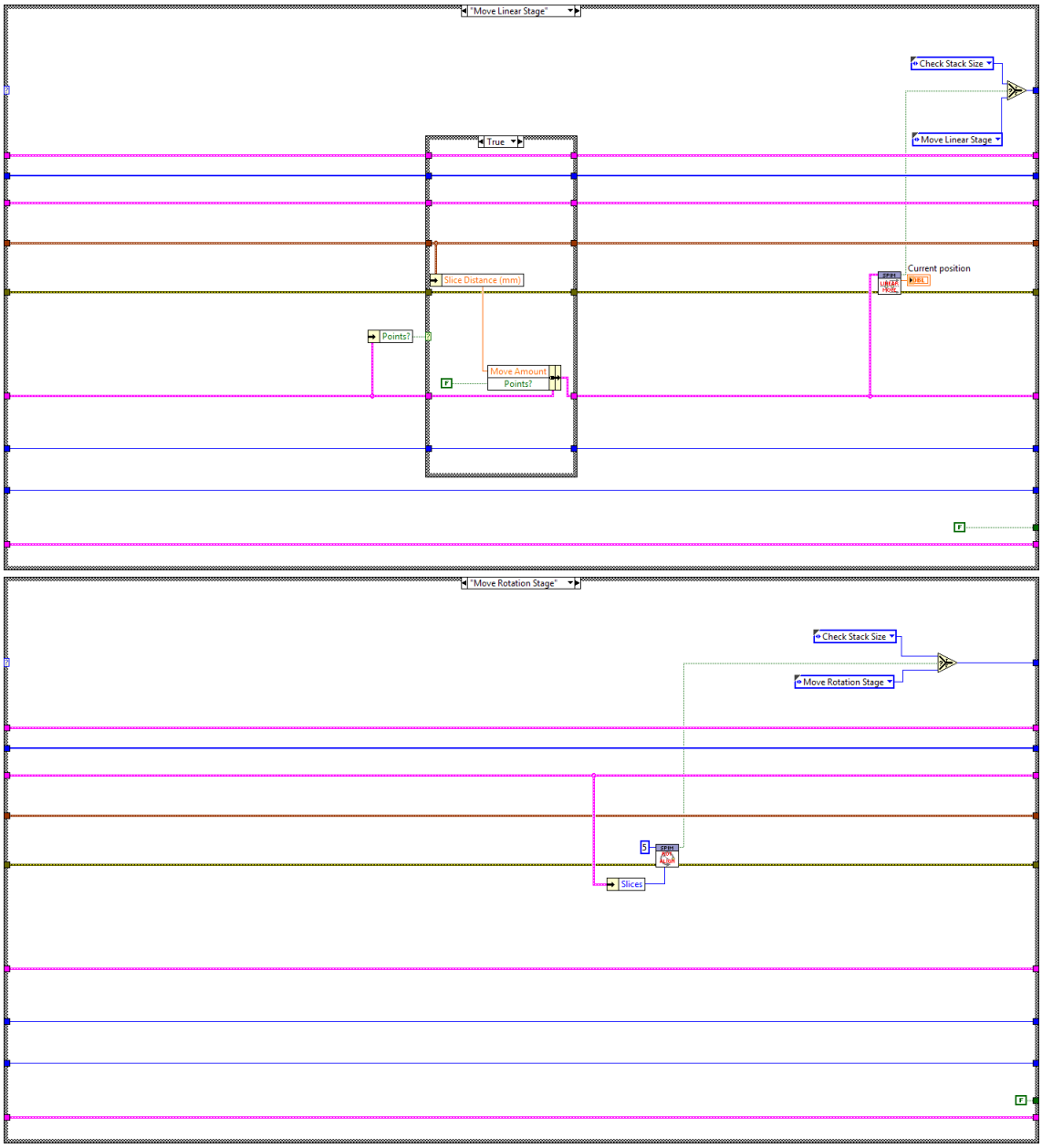
"Move Linear Stage"
Check Stack Size
Move Linear Stage
True
Slice Distance (mm)
Current position
Points?
Move Amount
Points?
"Move Rotation Stage"
Check Stack Size
Move Rotation Stage
5
Slices

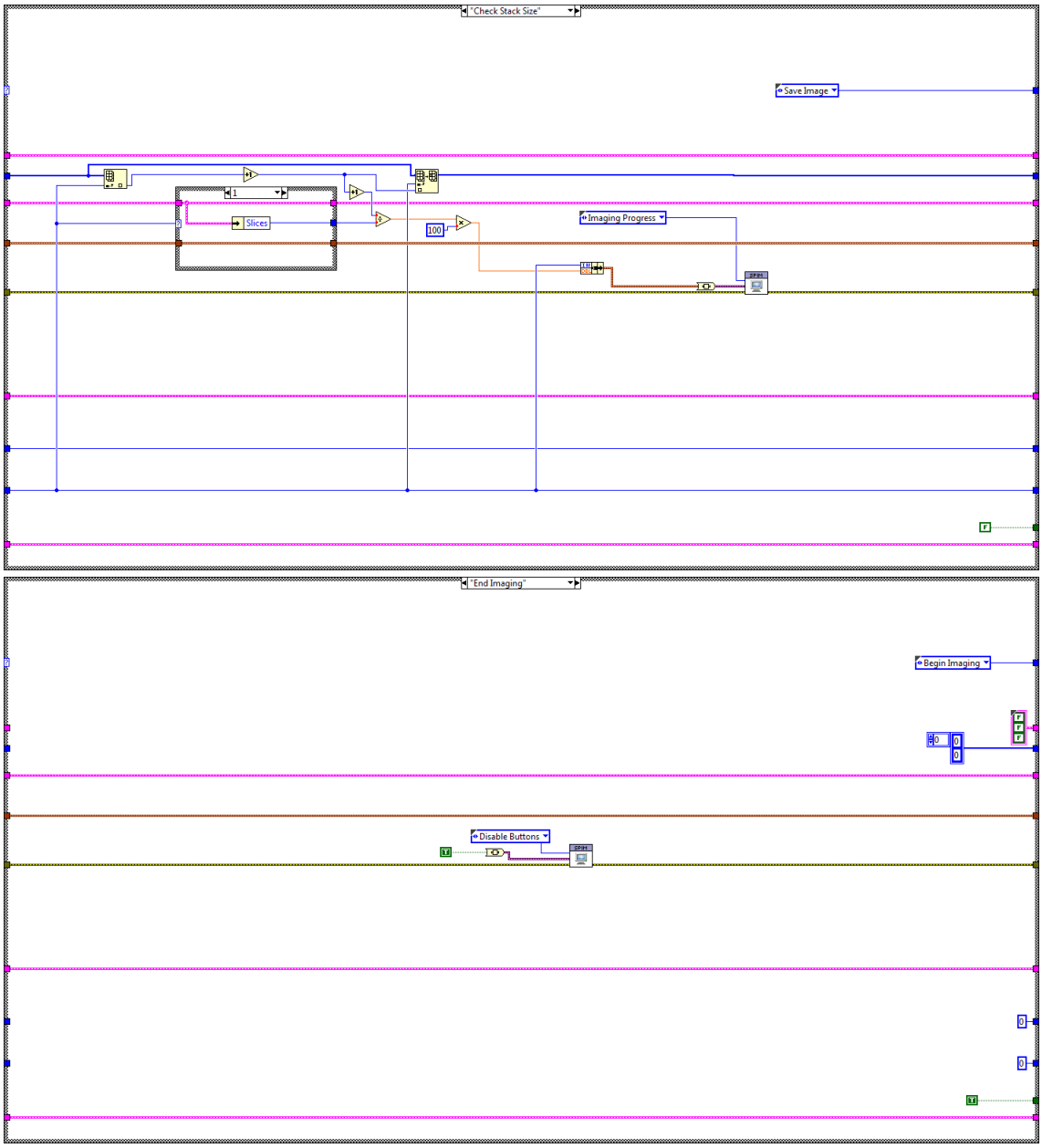

Figure 22. *State machine inside the Image-subroutine*